Combined toxicity of graphene oxide and wastewater to the green alga *Chlamydomonas reinhardtii*

Please, cite as follows:

Idoia Martín-de-Lucía, Marina C. Campos-Mañas, Ana Agüera, Francisco Leganés, Francisca Fernández-Piñas, and Roberto Rosal. Combined toxicity of graphene oxide and wastewater to the green alga *Chlamydomonas reinhardtii*. Environ. Sci.: Nano, 5, 1729-1744, 2018.
https://doi.org/10.1039/C8EN00138C

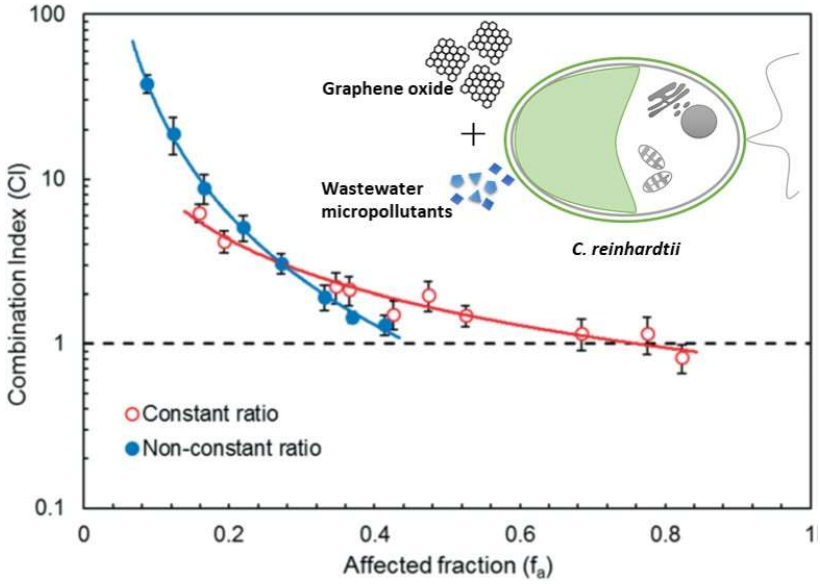

https://pubs.rsc.org/en/content/articlelanding/2018/en/c8en00138c

Combined toxicity of graphene oxide and wastewater to the green alga *Chlamydomonas reinhardtii*

Idoia Martín-de-Lucía[1], Marina C. Campos-Mañas[2], Ana Agüera[2], Francisco Leganés[3], Francisca Fernández-Piñas[3], and Roberto Rosal[1,†]

[1] Department of Analytical Chemistry, Physical Chemistry and Chemical Engineering, University of Alcalá, Alcalá de Henares, E-28871 Madrid, Spain

[2] CIESOL, Joint Centre of the University of Almería-CIEMAT, La Cañada de San Urbano, 04120 Almería, Spain

[3] Department of Biology, Faculty of Science, Universidad Autónoma de Madrid, E-28049, Spain

[†] Corresponding author: roberto.rosal@uah.es

Abstract

The toxic action of graphene oxide (GO) and the micropollutants contained in a biologically-treated wastewater were studied alone and in combination. For the toxicity assays, the unicellular green alga *Chlamydomonas reinhardtii* was used and the toxic mechanism was assessed by studying changes in esterase activity, cytoplasmic membrane potential, membrane integrity, the generation of intracellular reactive oxygen species (ROS), changes in intracellular calcium, mitochondrial membrane potential, and mitochondrial ROS formation. The joint toxic effect was quantified using the Combination Index (CI)-isobologram method using 72 h growth rate data. The pollutants monitored were polar pharmaceuticals, metabolites, and artificial sweeteners with concentrations from tens of ng L^{-1} to several μg L^{-1}. The amount of compounds adsorbed on GO reached 89.5 μg g^{-1} with preferential adsorption for the more hydrophilic. The most adsorbed compounds were azithromycin, clarithromycin, erythromycin, metoclopramide, ofloxacin, and ranitidine. GO induced cell damage due to oxidative stress. Short-term defence response was observed consisting of an increase in intracellular calcium levels and higher metabolic activity. Long-term damage was evidenced by mitochondrial ROS increase and strong depolarisation of the mitochondrial membrane. Cells exposed to GO-wastewater mixtures were considerably less affected with lower or non-significant damage in comparison with GO or wastewater alone. GO-wastewater mixtures displayed considerable antagonism for the lower values of assayed concentrations. The antagonism was attributed to the adsorption of toxic chemicals on the surface of GO nanoparticles and to the higher aggregation of GO in wastewater. The results show that non-additive interactions at low effect levels cannot be generally neglected.

1. Introduction

The presence of emerging anthropogenic pollutants in wastewater discharges has been extensively reported [1, 2]. They represent a diverse group of chemicals with incipient regulatory status and whose long-term effects are still unknown [3]. There are many complications for the risk assessment of wastewater-driven emerging pollutants, such as the difficulty to establish reliable removal rates in wastewater treatment plants [4]. Another relevant fact is that emerging pollutants are usually present in complex mixtures and mixture toxicity is still difficult to integrate into regulatory frameworks [5]. The prediction of mixture toxicity has been addressed by numerous studies, many of which support the additivity paradigm, where chemicals with the same mode of action can be described as a single component by adding-up their potency-corrected concentrations. According to mainstream opinion, the toxicological interactions of chemicals at the low concentrations usually found in water bodies would be negligible [6]. However, it has been suggested that the supposed low incidence of toxicological interactions might simply be a consequence of the lack of sufficient experimental evidence, with the frequency that non-additive interactions occur in environmental organisms being essentially unknown [7, 8].

The increased use of nanomaterials unavoidably results in their occurrence in waste streams, including treated wastewater and the sludge of wastewater treatment plants [9]. The presence of engineered nanoparticles in environmental compartments supposes an important alteration of aquatic colloids, which strongly affect the fate and behaviour of trace anthropogenic pollutants via physical and chemical interactions [10]. It has been shown that the adsorption of biomolecules on nanoparticles alter their physicochemical properties resulting in new potential impacts for living cells [11]. However, the interaction of nanoparticles with aqueous pollutants is still largely unknown. In a recent work, Martín-de-Lucía *et al*. reported a systematic antagonistic effect of wastewater micropollutants in the presence of metal oxide nanoparticles, which was attributed to the sequestration of pollutants due to adsorption on the nanoparticle surface [12]. In different situations, and concerning carbon based nanoparticles, either an

increase or a decrease in the toxicity of mixtures with respect to pure pollutants has been recorded [13, 14].

Graphene oxide (GO) is produced by chemical oxidation of graphite. The introduction of oxygenated functional groups leads to the exfoliation of the graphite structure ultimately producing a monolayer or a few-layers material [15]. GO is a convenient intermediate for preparing other graphene materials and the presence of hydrophilic functional groups allows easy dispersion into water and polar solvents [15]. It has been shown that GO is toxic for microorganisms, a property used to prepare antibacterial and biofilm-resistant surfaces [16]. GO interaction with environmental organisms has been less studied and the available information is still incomplete on aspects such as internalization and the nature of damage produced to cell membranes [17].

In this work, we studied the combined toxicity of GO and the pollutants of a real treated wastewater. We studied the adsorption of wastewater micropollutants on GO and assessed the effect of GO, wastewater and their mixtures on the growth of the green alga *Chlamydomonas reinhardtii*. The interactions were assessed by means of the combination index (CI)-isobologram equation [18]. The mechanistic effects of GO, wastewater and GO-wastewater mixtures on *C. reinhardtii* cells were assessed by studying changes in esterase activity, cytoplasmic membrane potential and integrity, the production of intracellular reactive oxygen species (ROS), changes in intracellular free Ca^{2+}, mitochondrial membrane potential, and mitochondrial ROS formation.

2. Experimental section

2.1. Materials

High purity analytical standards from Sigma-Aldrich (Steinheim, Germany) were used in this study. All reference standards presented a purity higher than 97%. Individual stock standard solutions were prepared at 1000 mg L^{-1} in methanol (MeOH) or acetonitrile (AcN) and stored in amber glass vials at −20 ˚C. Multi-compound working solutions containing all analytes were prepared by appropriate mixture and dilution of the stock standard solutions and were used for spiking samples in the quantifying procedure. AcN and MeOH HPLC grade, formic acid (98%), sodium hydroxide (NaOH > 99%) and dimethyl sulfoxide (DMSO > 99.9%) were supplied by Fluka (Buchs, Germany). Ultrapure water was generated from a Direct-Q^{TM} Ultrapure Water System from Millipore (Bedford, MA, USA) with a specific resistance of 18.2 MΩ cm^{-1} and total organic carbon (TOC) of 2 mg L^{-1}. Fluorescein diacetate (FDA), 2′,7′-dichloroflurescein diacetate (H_2DCFDA), C4-BODIPY®, propidium iodide (PI), bis-(1,3-dibutylbarbituric acid) trimethine oxonol ($DiBAC_4(3)$), 5,5′,6,6′-tetrachloro-1,1′,3,3′-tetraethyl-benzimi-dazolylcarbocyanine iodide (JC-1), MitoTracker Orange CM-H2 TM ROS and Calcium Green-1 AM were acquired from Thermo Fisher, USA.

Graphene oxide (GO, 2 mg mL^{-1} in H_2O) was obtained from Sigma-Aldrich. The characterization of GO suspensions was performed in ultrapure water, algal medium and wastewater. GO stocks (100 mg L^{-1}) were prepared using a Sonics VibraCell ultrasound disperser (BioBlock Scientific, France) operating at 500 W, as explained below. The particle size distribution and ζ-potential of GO suspensions were measured by dynamic light scattering (DLS) and electrophoretic light scattering, respectively using a Zetasizer Nano ZS instrument (Malvern Instruments Ltd) at 25 ˚C.

The wastewater sample was collected from the secondary clarifier of a wastewater treatment plant (WWTP) located in Madrid, which treats a mixture of domestic and industrial wastewater with a nominal capacity of 13000 m^3/h. Wastewater was filtered using 0.45 μm PTFE filters and kept frozen (-20 °C) in glass bottles and in the dark until runs and analyses. Before the experiments the samples were redispersed to ensure homogeneity. The pH of wastewater immediately before runs was 6.5, as shown in Table S1 (Electronic Supplementary Information) together with its main characterization parameters.

2.2. Analysis of micropollutants

Wastewater and GO (10 mg L^{-1} and 100 mg L^{-1}) were put in contact in dark flasks at pH 6.5 and 20 ˚C under constant stirring in the dark to avoid photochemical reactions and the production of oxidation intermediates from wastewater micropollutants. After 24 h the suspensions (20 mL aliquots) were filtered using Vivaspin 20, 5 kDa, polyethersulfone ultrafiltration centrifuge tubes and the filter content after filtering was washed twice with methanol (2 mL + 2 mL) as described elsewhere [12].

The detection and quantification of micropollutants was carried out in: i) raw wastewater, ii) ultra-filtered wastewater, before and after contact with GO, and iii) in the two extractions with methanol. Analyses were performed by high-performance liquid chromatography coupled with mass spectrometry, using a triple quadrupole-linear ion trap analyser (HPLC-QqLIT-MS/MS). The instrumentation consisted of an Agilent 1200 LC system (Agilent Technologies, Foster City, CA, USA) and a 5500 QTRAP analyser (AB Sciex Instruments, Wilmington, DE, USA). The chromatographic separation was carried out with a ZORBAX Eclipse XDB C18 analytical column (50 mm x 4.6 mm i.d, 1.8-μm particle size). Mobile phases were 0.1% formic acid in water (eluent A) and acetonitrile (AcN, eluent B), and gradient conditions were as described by Campos Mañas et al. [19]. Analysis was performed by direct injection of the samples (10 μL). Pre-treatment was limited to the addition of AcN to obtain the same proportion of AcN:H_2O (10:90, v/v) as

the initial conditions of the chromatographic method. The MS was operated in the selected reaction monitoring (SRM) mode with Schedule MRM™ Algorithm to improve sensitivity of the analytical method. MS operating conditions were also optimized as described elsewhere [19]. The optimized method provided low limits of detection (< 100 ng L^{-1}) and quantification (< 500 ngL^{-1}) and mean recoveries in the range of 70-120% with precision values ≤ 25%, for most compounds.

2.3. Microalgal cultures and algal growth bioassays

The unicellular green alga *Chlamydomonas reinhardtii* was routinely cultured in 250 mL Erlenmeyer flasks in 100 mL of Tris-minimal phosphate (TP) medium at pH 6.5 and 28 ± 1 ˚C under continuous illumination using a rotatory shaker at 135 rpm [20]. Algal cells were exposed up to 72 h to different concentrations (0.05, 0.1, 0.5, 1, 5, 10, 25, and 50 mg L^{-1}) of GO and to wastewater dilutions in the 0.198-1 range. Fresh stocks of GO suspension were prepared in TP medium a few minutes before every toxicity assays to ensure the homogeneity of stock suspension and to prevent undesired ageing or aggregation. The stock suspension was dispersed using a Sonics VibraCell ultrasound disperser (BioBlock Scientific, France) for 30 min and subsequently diluted in TP medium to obtain the appropriate concentrations. Wastewater was serially diluted (dilution factor of 1.5) with tenfold concentrated TP medium.

For the toxicity bioassays, *C. reinhardtii* cultures were washed twice and resuspended in fresh TP medium to obtain an initial optical density (OD_{750nm}) of 0.1. The assays were carried out in 14 mL of TP medium in 25 mL Erlenmeyer flasks and cultures were exposed to GO suspensions and wastewater for up to 72 h in a rotatory shaker at 135 rpm, 28 °C, and constant illumination with 40 µmol photons m^2 s^{-1}. Exposure experiments were performed in three independent sets with triplicate samples and non-exposed cultures as controls. OD_{750nm} of algal cell cultures was measured daily (0, 24, 48 and 72 h) by transferring 250 µL (duplicate samples) to 96-well transparent microplates. The readings were performed on a Synergy HT multimode microplate reader (BioTek, Seattle, WA).

Growth inhibition (%) after 72 h exposure was calculated for each GO concentration and for each wastewater dilution tested. EC_{50} (the median effective concentration of GO or wastewater dilution that causes 50% of growth inhibition with respect to a non-treated control) values of dose-response curves of GO and wastewater were fitted by non-linear parametric functions with the statistical software R "drc" analysis package (RStudio for Windows) [21]. The four-parameter log-logistic model (LL.4, drc) was selected for fitting the dose-response curves. EC_{50} value and 95% confidence interval values were computed using the function ED.drc (drc) on fitted LL.4 models [22].

2.4. Mixture toxicity bioassays

For evaluating the nature of the interaction of GO with wastewater, binary combinations of GO and wastewater (GO-wastewater) were prepared and tested for *C. reinhardtii*. Algal cells were treated with dilutions of GO and wastewater individually and in combinations prepared with a fixed constant ratio (1:1) based on the individual EC_{50} values and with a non-constant ratio based in the additivity line (the experimental design is shown in Fig. 1 and the values given in Table S2, ESI). Five dilutions (constant ratio: serial dilution factor of 1.7) of GO and wastewater and their combinations plus a control were tested in three independents experiments with triplicate samples as described in Table S2. All individual GO, wastewater and their combinations assays were carried out at the same time as recommended by Chou [23] to maximize computational analysis of data.

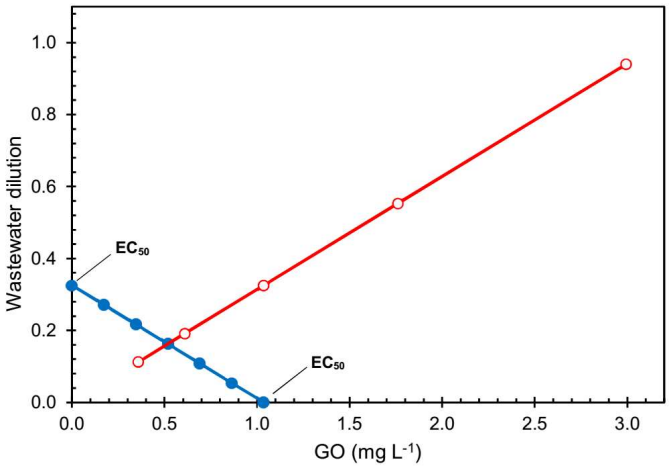

Figure 1. Experimental design for determining the binary combinations of GO and wastewater (WW) for *C. reinhardtii*. Constant ratio (○), and non-constant ratio (●).

The response to combined toxicities exposure in the *C. reinhardtii* test was estimating using the median-effect equation [18] based on the mass-action law:

$$\frac{f_a}{f_u} = \left(\frac{D}{D_m}\right)^m \quad (1)$$

where f_a is the fraction affected by a certain dose, D, and f_u the unaffected fraction ($f_a = 1 - f_u$), D_m representing the dose for 50% effect (median effect-dose, EC_{50}). m is the coefficient of the sigmoidicity of the dose-effect curve. $m = 1$, $m > 1$, and $m < 1$ indicate hyperbolic, sigmoidal, and negative sigmoidal dose-effect curve, respectively. Therefore, the method takes into account both the potency (D_m) and shape (m) parameters. Eq. 1 may be arranged as follows:

$$D = D_m \left(\frac{f_a}{1 - f_a}\right)^{1/m} \quad (2)$$

The D_m and m values for each individual nanoparticle and wastewater, or mixture were determined by the median-effect plot: x = log (D) versus y = log (f_a/f_u), which is based on the logarithmic form of Eq. (1). The

conformity of the data to the median-effect principle can be assessed by the linear correlation coefficient (r) of the data to the logarithmic form of Eq. 2. These parameters were then used to calculate doses of individual compounds and their combinations required to produce various effect levels according to Eq. (1). Combination index values (CI) for each effect level were calculated according to the general CI equation [23]:

$$^{n}(CI)_x = \sum_{j=1}^{n} \frac{(D)_j}{(D_x)_j} = \sum_{j=1}^{n} \frac{(D_x)_{1-n}\left(\frac{[D]_j}{\sum_1^n [D]}\right)}{(D_m)_j\left(\frac{(fa_x)_j}{[1-(fa_x)_j]}\right)^{1/mj}} \quad (3)$$

where $^{n}(CI)_x$ is the combination index for n chemicals at x% growth inhibition; $(D_x)_{1-n}$ is the sum of the dose of n chemicals that exerts x% growth inhibition in combination, $([D]_j / \sum_1^n [D])$ is the proportionality of the dose of each of n chemicals that exerts x% growth inhibition in combination; and $(D_m)_j (fa_x)_j / [1 - (fa_x)_j]^{1/mj}$ is the dose of each drug alone that exerts x% growth inhibition. From Eq. (3), CI < 1, CI = 1 and CI > 1 indicates synergism, additive effect and antagonism, respectively [23]. The data were analysed using the computer program CompuSyn to determine the dose-effect curve parameters and CI values of the different mixtures in the whole range of effect levels [24].

2.5. Mechanistic studies

Flow cytometry (FC) analyses of *C. reinhardtii* cells were performed on a Cytomics FL500 MPL flow cytometer (Beckman Coulter Inc., Fullerton, CA, USA) equipped with an argon-ion excitation wavelength (488 nm), a detector of forward scatter (FS), a detector of side scatter (SS), and with four fluorescence detectors corresponding to four different wavelength intervals: FL1: 525 nm, FL2: 575 nm, FL3: 620 nm, and FL4: 675 ± 20 nm. The 488 nm argon-ion laser was used as the excitation source for all the probes assayed. Relevant physiological parameters were determined using different functional fluorochromes.

Algal cells were exposed to 1.036 mg L^{-1} (EC_{50}) of GO, 5 mg L^{-1} of GO, 0.325 (EC_{50}) of wastewater effluent dilution, and to a binary combination of GO and wastewater with a fixed ratio (EC_{50} GO + EC_{50} wastewater: 1.036 mg L^{-1} + 0.325 wastewater dilution). After 1, 24 and 72 h of exposure, 200 µL samples of algal cultures were incubated with the appropriate fluorochrome as prescribed prior to FC analyses. Non-treated cells were diluted with culture medium to the same treated cells density. All fluorochrome stock solutions were prepared in dimethyl sulfoxide (DMSO) and stored at −20 °C, with the exception of the solution of propidium iodide (PI), which was prepared in Milli-Q water and stored at 4 °C, and the fluorochrome C4-BODIPY®, which was diluted in methanol.

Three independent experiments with triplicate samples were carried for each parameter. For all the cytometric parameters studied, at least 10^4 events (algal cells) per sample were counted and fluorescence (due to the presence of chlorophyll *a* and other pigments) was analysed in logarithmic mode. Forward scatter (FS) and red autofluorescence dot-plots were used to characterize the microalgal population. Cells were gated based on these parameters to exclude non-microalgal particles from the analysis.

The changes in cellular metabolic activity were evaluated using the FDA cytometric assay, based on esterase activity [28, 29]. FDA is a non-polar, non-fluorescent lipophilic molecule cleaved off by non-specific esterases giving rise to the green-fluorescent product fluorescein, which is retained by cells with intact plasma membranes. Algal cells were incubated with 0.1 µg mL^{-1} of FDA for 10 min at room temperature and in darkness conditions.

Intracellular ROS formation was detected using the fluorescent dye 2′,7′-dichloroflurescein diacetate (H_2DCFDA), which is transformed by intracellular H_2O_2 into the green-fluorescent 2′,7′-dichloroflurescein (DCF). Algal cells were incubated with 48 µg mL^{-1} H_2DCFDA in the dark for 30 min at room temperature. A positive control incubated with 0.1 mM of H_2O_2 was also tested.

Lipid peroxidation was evaluated using the fluorochrome C4-BODIPY®, which is oxidized by peroxyl radicals, producing green fluorescence. *C. reinhardtii* cells were incubated for 10 min at room temperature with a final concentration of C4-BODIPY® of 2 µg mL^{-1}.

Cytoplasmic membrane integrity was assessed using the Propidium iodide (PI) permeability bioassay. PI is unable to pass through intact cell membranes but can penetrate the cells if the integrity of the membrane is altered and intercalated with double-stranded nucleic acids, resulting in high fluorescence intensity. Algal cells were incubated with 2.5 µg mL^{-1} of PI for 10 min [25], at room temperature and in darkness conditions.

The alterations of cytoplasmic membrane potential were studied using the lipophilic anionic oxonol dye $DiBAC_4(3)$ that can enter depolarised cells where it binds to intracellular proteins [26]. Depolarisation of cell membranes increases green fluorescence (increase of intracellular anionic dye concentration), conversely, hyperpolarisation decreases fluorescence. *C. reinhardtii* cells were incubated with 0.5 µg mL^{-1} of $DiBAC_4(3)$ for 10 min.

The changes in mitochondrial membrane potential were evaluated by means of the lipophilic cationic fluorochrome 5,5′,6,6′-tetrachloro-1,1′,3,3′-tetraethyl-benzimi-dazolylcarbocyanine iodide (JC-1). JC-1 exhibits potential-dependent accumulation in mitochondria with fluorescence emission shifting from green (monomer) to red (aggregates). Mitochondrial depolarisation decreases the red/green fluorescence

intensity ratio. Cell suspensions were incubated with 5 μg mL^{-1} JC-1 for 20 min.

Mitochondrial ROS were assessed by MitoTracker Orange CM-H2 TM ROS, an orange-fluorescent dye that stains mitochondria in live cells, the accumulation of which depends on membrane potential and fluoresces upon oxidation. *C. reinhardtii* cells were incubated for 1h with 0.2 μg mL^{-1} MitoTracker Orange CM-H2 TM ROS.

Cytoplasmic intracellular free Ca^{2+} ($[Ca^{2+}]_c$) was analysed using Calcium Green-1 AM, which diffuses freely into the cells, where non-specific esterases cleave acetate group and Calcium Green-AM binds to intracellular free Ca^{2+} leading to an increase in green fluorescence. *C. reinhardtii* cells were incubated with 12.9 μg mL^{-1} Calcium Green-1 AM for 2 h.

FC data were collected using MXP software and analysed using Flowing Software 2.5.1. To determine significant differences, FC data were statistically analysed using R software 3.3.3. (The R Foundation for Statistical Computing) and Rcmdr 2.3–2 package [27]. A one-way ANOVA coupled with Tukey's HSD (honestly significant difference) post-hoc test was performed for comparison of means. Statistically significant differences were considered to exist when p-value < 0.05.

2.6. Transmission electron microscopy

High-resolution transmission electron microscopy (TEM) images of *C. reinhardtii* cells exposed to 1.036 mg L^{-1} (EC_{50}) and 5 mg L^{-1} of GO, to 0.325 (EC_{50}) of wastewater dilution, and to binary combinations with a fixed ratio (EC_{50} GO:EC_{50} wastewater) were taken on a JEOL JEM 1400 microscope operating at 100 kV. After 72 h of exposure, 14 mL of non-exposed cells (control) and treated cultures were centrifuged, and the supernatant discarded. Without disturbing the pellet, cells were washed with 1 mL of washing buffer (0.1 M cacodylate, pH 7.2). The washing buffer was removed, and 1 mL of fixation buffer (2.5 % glutaraldehyde in 0.1 M wash buffer) was added. Cells were fixed for 6 h at 4 °C. After fixation, the samples were washed three times for 10 min with the washing buffer and kept at 4 °C overnight. Postfixation was in 1% osmium tetroxide in washing buffer for 1 h at room temperature. Then, the pellet was rinsed with dH_20 three times for 10 min and dehydrated with increasing concentrations of acetone (30-50-70-80-90-95-100 %) for 15 min. Dehydrated samples were infiltrated and embedded with Spurr-resin at room temperature by increasing resin concentrations in acetone: 1:3 (1 h), 1:1 (1 h), and 3:1 (2 h). The samples were subsequently placed in pure resin at room temperature overnight. Finally, resin polymerization took place at 60˚C for 48 h. The sectioned samples in semi-thin (0.5 μm) and ultra-thin sections (60 nm) were stained with uranyl acetate and lead citrate.

3. Results and discussion

3.1. GO Characterization

The physicochemical properties of GO dispersions in pure water at pH 6.5, TP medium (the experimental medium used for toxicity experiments), and wastewater are shown in Table 1 for freshly prepared mixtures and after 24 h and 72 h. The hydrodynamic diameter measured by DLS revealed the presence of aggregates of several hundreds of nanometres. In wastewater, the size of particle aggregates increased with the addition of GO over the colloidal background and with time. In TP, however, the aggregates showed a tendency to decrease with contact time, which was probably a consequence of the colloidal stability imparted by GO as revealed by the negative ζ-potential of particles. The effect of GO on the surface charge of suspended particles was lower in wastewater due to the higher concentration of background colloidal particles and only at concentrations as high as 100 mg L^{-1} of GO in wastewater, the ζ-potential at pH 6.5 of the colloid was significantly more negative than that of raw wastewater. For higher GO concentrations, lower aggregates were also observed, in the 50-200 nm range, which were most probably in dynamic equilibrium with the larger ones.

3.2. Micropollutant adsorption studies

Up to 33 organic micropollutants could be identified in the samples by the analytical method proposed. These compounds are mainly polar pharmaceuticals, belonging to different therapeutic groups, some of their metabolites and artificial sweeteners. The lower concentrations were measured for diazepam, indomethacin, and metoprolol, in the tens of ng L^{-1} range and the higher, in the few μg L^{-1} range, for 4-formyl-aminoantipyrine (4-FAA), antipyrine, gemfibrozil, hydrochlorothiazide and sucralose. The concentration of detected pollutants in raw wastewater was in the tens of ng L^{-1} to several μg L^{-1} range and is listed in Table S3 (ESI) together with their main physicochemical properties.

Fig. 2 shows the amount adsorbed on GO after 24 h in contact with wastewater for the two tested GO concentrations. The total concentration of compounds for which the concentration measured in wastewater before and after adsorption was statistically significant amounting to 89.5 μg g^{-1} for GO 10 mg L^{-1} and 29.5 μg g^{-1} for GO 100 mg L^{-1}. This amount of adsorbed compounds corresponded to 3.7 % for GO 10 mg L^{-1} and 12.1 % for GO 100 mg L^{-1} of the total amount of the quantified pollutants (the list of 33 compounds included in Table S3). The fact that the adsorbed amount of the analysed compounds per unit mass of GO was not linear with GO concentration can be attributed to the depletion of organic pollutants from wastewater between these two concentrations. Besides, the presence of other compounds in wastewater (NPOC was 17 mg L^{-1}), dominated by hydrophilic organic matter competed with the analysed pollutants for the adsorption centres of GO[28]. Considering individual compounds, the highest

Table 1. Physicochemical properties of GO, 10 mg L^{-1} in ultrapure water, TP medium and wastewater.

	Water, pH 6.5		Wastewater, pH 6.5		Tris-minimal phosphate medium, TP, pH 6.5	
	ζ-potential (mV)	d_{DLS} (nm)	ζ-potential (mV)	d_{DLS} (nm)	ζ-potential (mV)	d_{DLS} (nm)
Without GO			-18.1 ± 0.6	518 ± 43	-17.4 ± 1.2	411 ± 28
GO 10 mg L^{-1} (0 h)	-32.8 ± 0.8	276 ± 24	-18.6 ± 0.9	617 ± 67	-27.9 ± 2.3	756 ± 54
GO 10 mg L^{-1} (24 h)	-33.6 ± 0.5	252 ± 6	-16.3 ± 0.6	1008 ± 120	-27.5 ± 1.8	681 ± 107
GO 10 mg L^{-1} (72 h)	-35.7 ± 0.8	277 ± 1.2	-17.8 ± 1.2	1355 ± 264	-23.9 ± 0.2	542 ± 162
GO 100 mg L^{-1} (0 h)	-33.5 ± 1.9	332 ± 36	-20.4 ± 1.2	1720 ± 106	-30.3 ± 1.4	804 ± 63
GO 100 mg L^{-1} (24 h)	-33.1 ± 0.8	266 ± 12	-19.9 ± 1.0	1380 ± 69	-32.2 ± 1.2	978 ± 72
GO 100 mg L^{-1} (48 h)	-37.2 ± 0.5	263 ± 15	-18.7 ± 2.1	1288 ± 58	-30.4 ± 0.4	857 ± 64

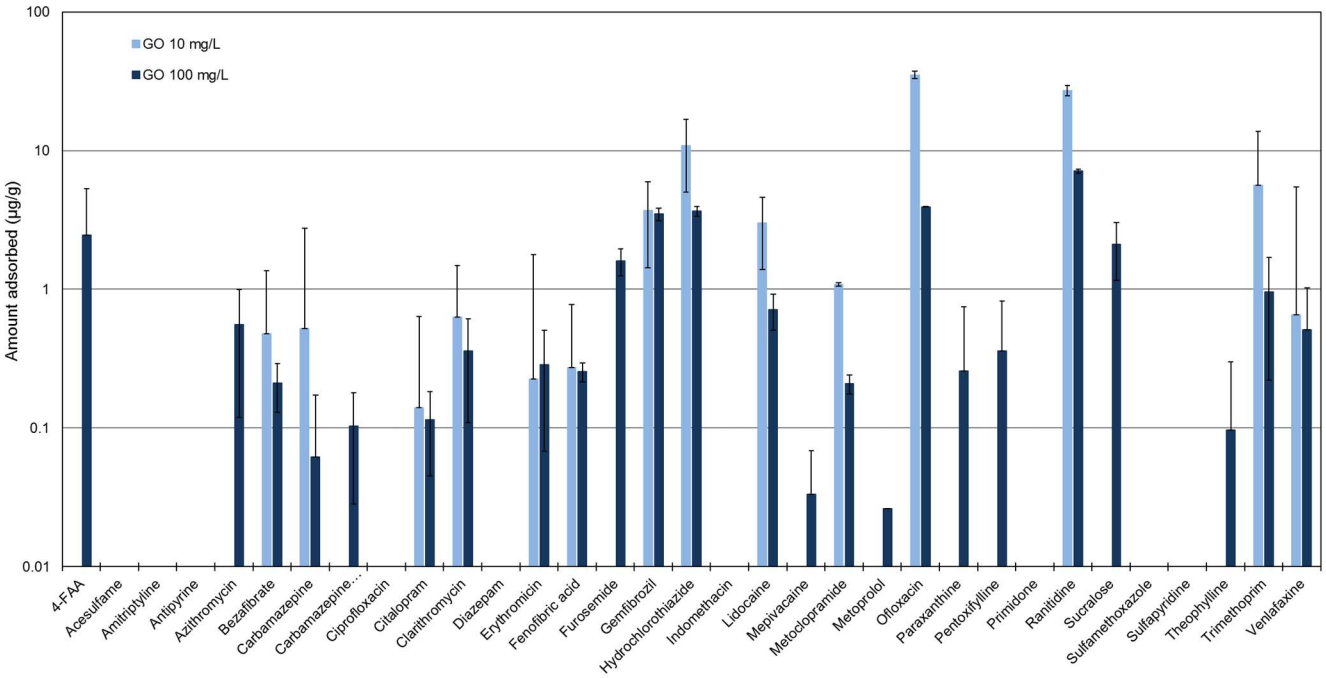

Figure 2. Amount of pollutants adsorbed on GO after 24 h in contact with wastewater. (Error bars are standard deviations of two assays with duplicated analyses.)

amounts adsorbed corresponded to: gemfibrozil (3.7 ± 2.3 µg g^{-1}), hydrochlorothiazide (10.9 ± 5.9 µg g^{-1}), lidocaine (3.0 ± 1.6 µg g^{-1}), ofloxacin (35.1 ± 2.1 µg g^{-1}), ranitidine (27.1 ± 2.3 µg g^{-1}), and trimethoprim (5.6 ± 8.1 µg g^{-1}) for 10 mg g^{-1} GO, all of them above the threshold of 1 µg g^{-1}. The compounds with highest amount adsorbed in the GO 100 mg L^{-1} suspension were essentially the same: furosemide (1.6 ± 0.4 µg g^{-1}), gemfibrozil (3.5 ± 0.8 µg g^{-1}), hydrochlorothiazide (3.7 ± 0.3 µg g^{-1}), ofloxacin (3.9 ± 0.2 µg g^{-1}), and ranitidine (7.1 ± 0.2 µg g^{-1}). Relative to their occurrence in wastewater, the most retained compounds were metoclopramide (22 %), ofloxacin (75 %) and ranitidine (32 %) for 10 mg L^{-1} GO, and azithromycin (27 %), clarithromycin (22 %), erythromycin (21 %), metoclopramide (42 %), ofloxacin (83 %) and ranitidine (83 %) for 100 mg L^{-1} GO.

Fig. S1 (ESI) shows the amount recovered for each compound after two consecutive washings with methanol of the Vivaspin, 5 kDa, polyethersulfone filters. Some compounds could be recovered at near 100 %, but, significantly, some others were strongly retained on the nanoparticle surface. These were azithromycin, citalopram, clarithromycin, ofloxacin, and ranitidine for which the recovery was below 50 % for at least one GO concentration. The results showed that as much as 74% (10 mg L^{-1} GO) or 81 % (100 mg L^{-1} GO) of ofloxacin remained on GO surface after two consecutive extractions, with values over 20 % for 10 out of the 33 compounds quantified. In other words, the adsorption was relatively strong for some compounds. To gain further insight on this subject, the amount adsorbed of the different compounds was plotted as a function of their octanol-water partition coefficient, K_{ow}, and their apparent or pH-dependant octanol-water partition coefficient, D_{ow}. K_{ow} and D_{ow} differ because D_{ow} considers the ionization constant of acidic or basic compounds according to their pK_a by means of the Henderson–Hasselbalch equations. The difference

between K_{ow} and D_{ow} and the derivation of D_{ow} has been reported in detail elsewhere [12]. Fig. 3 shows the cumulative amount of compounds significantly adsorbed onto GO at the two tested concentrations as a function of their log D_{ow} values. D_{ow} is a measure of the tendency of a given compound to partition between organic and aqueous phase at pH 6.5 in our case.

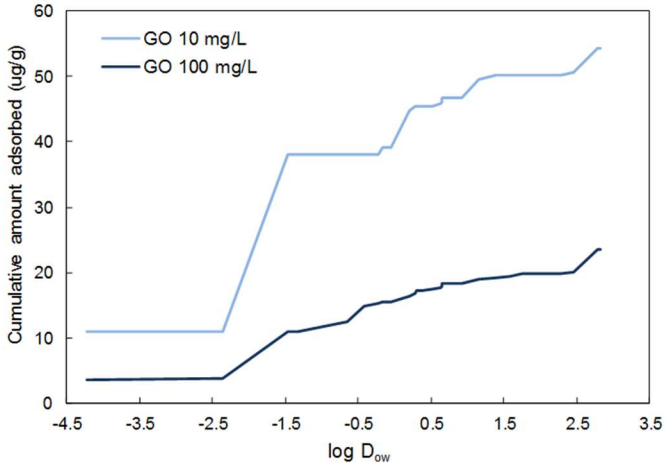

Figure 3. Cumulative amount of pollutants adsorbed on GO as a function of their apparent octanol-water partition coefficient, log D_{ow}. The reader is referred to Fig. S2 (ESI) for bubble plots graphically showing the compounds adsorbed in higher amounts.

The results showed a preferential adsorption capacity of GO for the more polar and hydrophilic compounds, which are those with low D_{ow} values. This result is consistent with the hydrophilic nature of GO, which is a consequence of the presence of oxygenated graphene sheets covered with epoxy, hydroxyl, and carboxyl groups. Therefore, GO showed preferential affinity towards the more hydrophilic compounds among those tracked in this work [29]. The result is particularly relevant considering many emerging pollutants are hydrophilic and show high mobility in aqueous environments [30]. Fig. S2 (ESI) illustrates the adsorption of individual compounds as bubbles proportional to the amount adsorbed and as a function of D_{ow} and K_{ow} showing that the polar compounds ranitidine and hydrochlorothiazide were the most strongly adsorbed on GO surface.

3.3. Effects on algal growth

The growth inhibition of *C. reinhardtii* after 72 h exposure was studied to assess the toxic effects of GO and wastewater. Fig. 4 shows both concentration-response relationships. The maximum growth inhibition for the green alga after 72 h in contact with GO was 85.9 ± 1.7 % at the highest tested concentration (50 mg L^{-1}). Wastewater toxicity is given as a dilution factor (where 1 corresponds to undiluted wastewater) and the maximum growth inhibition corresponded to undiluted wastewater: 80.9 ± 1.5 %. The maximum dilution tested (0.198) yielded 36.4 ± 3.1 % growth inhibition with no evidence of hormetic effect or grown stimulation.

The individual toxicities of GO and wastewater on growth of *C. reinhardtii* at 72 h exposure time are listed in Table S4 (ESI) as effective concentration (EC_x) of GO or the wastewater dilution that causes 20 %, 50 %, and 80 % growth inhibition with respect to a non-treated control (EC_{20}, EC_{50} and EC_{80}, respectively). The exposure to GO resulted in EC_{50} 1.04 (0.93-1.15) mg L^{-1} for the growth rate of *C. reinhardtii*. Up to our knowledge no results have been published for *C. reinhdartii* exposed to GO. As a reference, we included in Table S5 (ESI) a list of the ecotoxicological effects reported in the literature for GO on other photosynthetic microalgae. The EC_{50} for wastewater was 0.33 (0.31-0.34) dilution due to the high toxicity of untreated wastewater (> 80 % growth inhibition).

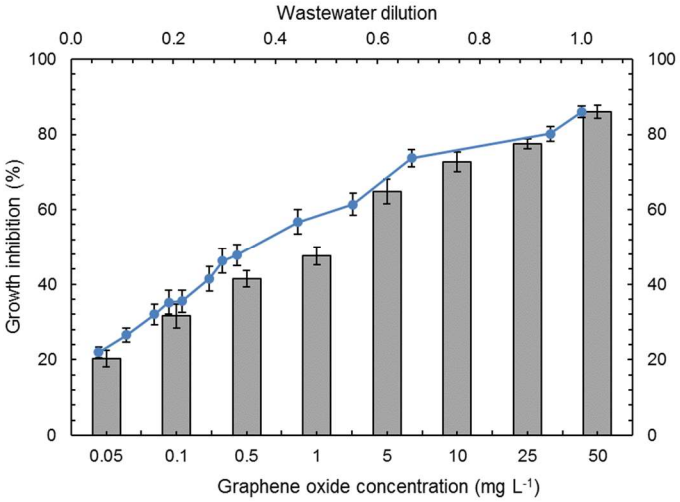

Figure 4. Growth inhibition of *C. reinhardtii* as a function of GO concentration (bars, lower scale) and wastewater dilution (●, upper scale) after 72 h exposure. (Error bars represent standard deviation, n = 9.)

3.4. Toxicity of binary mixtures

Fig. 5 shows the f_a-CI plots for both types of mixtures after 72 h exposure of *C. reinhardtii* to binary mixtures composed of GO and wastewater in constant and non-constant ratios as indicated before. CI values were plotted as a function of the fractional inhibition of growth within the experimental range of growth inhibition. The behaviour was very similar, with GO-wastewater combinations displaying antagonism over practically the whole experimental range of effect levels but approaching additivity for the highest affected fraction values (roughly above 0.5). For non-constant ratio, the binary combination of GO and wastewater for the lower values of affected fraction, corresponding to the less toxic mixtures, showed strong antagonism (CI > 10), with a tendency towards additive effect for the most toxic mixtures.

Table S6 (ESI) shows the dose-effect curve parameters (D_m, m and r) of GO and wastewater tested on *C. reinhardtii* 72h toxicity test singly and in their binary mixtures. Significantly, the shape of the dose-effect curve changes from hyperbolic or flat sigmoidal for

individual GO and wastewater to clearly sigmoidal for the binary mixtures.

3.5. Mechanisms of toxic action

The metabolic activity of cells was studied by measuring the esterase activity using the FDA flow

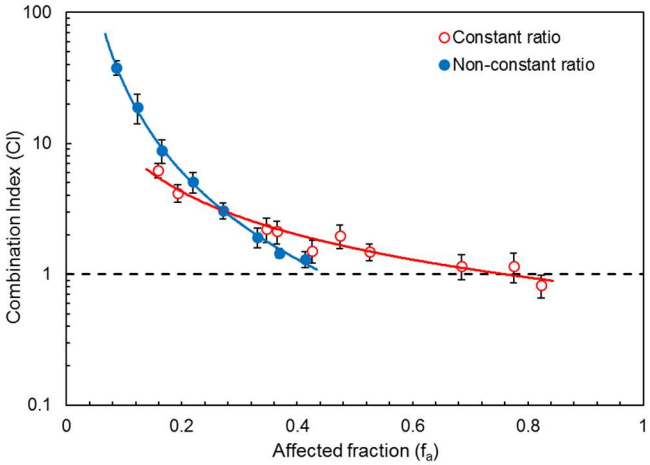

Figure 5. Combination index plot for binary combinations GO-wastewater. Constant ratio (○), and non-constant ratio (●). CI values are plotted as a function of the fractional inhibition of growth inhibition (f_a) within the experimental range. CI > 1 indicates antagonism and the dashed line additivity (CI = 1). Exposure time: 72 h. (Error bars represent standard deviation.)

cytometric assay (Fig. 6). After 1 h of exposure of *C. reinhardtii* to GO and to wastewater, esterase activity significantly increased ($p < 0.05$, roughly +10 % over controls). GO-wastewater binary combinations also increased ($p < 0.01$) metabolic activity about +18 % with respect to control. The stimulation of metabolic activity has been reported in microalgae exposed to benzophenone-3 [31] and paraquat [25] and is considered a physiological adaptation to adverse environmental conditions. After 24 h and 72 h, however, the metabolic activity was significantly ($p < 0.01$ and $p < 0.001$, respectively) reduced by GO, wastewater and GO-wastewater mixture. The reduction of metabolic activity of *C. vulgaris* by GO has also been described by Hu *et al*. [32]. Other results also reported decreased metabolic activity of *C. reinhardtii* cells exposed to different pollutants [33, 34]. GO, Wastewater, and wastewater-GO mixtures induced a similar inhibition of metabolic activity with confidence intervals overlapping except for 1 h contacts, for which we observed metabolic stimulation.

FC analyses based on red autofluorescence of the chlorophyll *a* are shown in Fig. S3 (ESI). At 24 h of exposure, a decrease in percentage of the chlorophyll *a* autofluorescence intensity was clear at 5 mg L^{-1} GO, whereas after 72 h exposure, there was no significant effect. No changes were observed in *C. reinhardtii* cells exposed to the EC_{50} GO. Several studies reported a decrease in the percentage of chlorophyll *a* autofluorescence intensity in the presence of GO [35].

The decrease of chlorophyll *a* fluorescence is usually explained as a consequence of oxidative stress [36] or by "shading effect" due to GO agglomeration in algal cultures [37]. Nevertheless, Tang *et al*. found that a GO concentration of 15 mg L^{-1} was required to significantly decrease chlorophyll *a* content [38]. On the other hand, after 24 h of exposure, the wastewater and GO-wastewater mixture caused a significant ($p < 0.01$) decrease in chlorophyll autofluorescence in line with results reported with chemical pollutants [34, 39]. The mixture GO-wastewater resulted in lower reduction of the chlorophyll *a* autofluorescence intensity than GO or wastewater alone at the same concentrations.

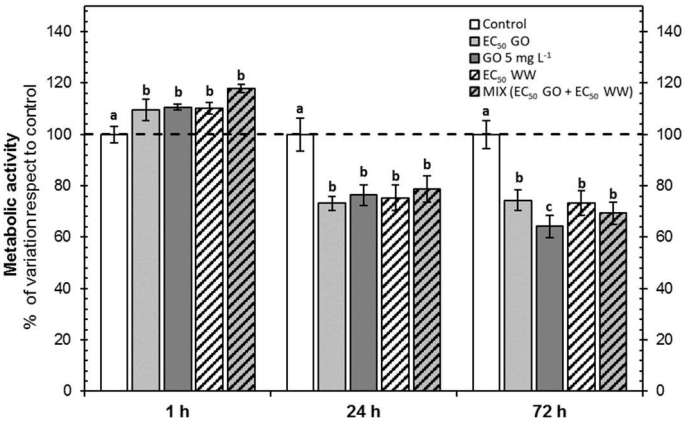

Figure 6. Variations in metabolic activity of *C. reinhardtii* cells by FC using the fluorochrome FDA after 1, 24 and 72 h of exposure. Results are shown as percentage of metabolic activity ± SD (n = 9) with respect to control (100% is indicated by the dashed line). Treatments with different letters are significantly different (Tukey's HSD, $p < 0.05$).

The effect of GO, wastewater and GO-wastewater mixtures on membrane integrity is shown in Fig. 7 based on PI exclusion. After 24 h of exposure cytoplasmic membrane integrity was significantly ($p < 0.01$) affected as revealed by an increase of PI fluorescence intensity. Cells exposed to wastewater also displayed increased PI fluorescence intensity with respect to control cells. After 72 h, cells' PI intensity decreased, possibly due to the action of calcium-mediated defence mechanisms (see below). The effect on cytoplasmic membrane potential of *C. reinhardtii*, studied using the fluorescent dye $DiBAC_4(3)$, is also shown in Fig. 7. Cells exposed to GO at its EC_{50} did not show any alterations and only cells exposed to 5 mg L^{-1} of GO induced a significant ($p < 0.05$) increase in $DiBAC_4(3)$-derived fluorescence emission. This result means that GO membrane interaction results in membrane depolarisation, even if the probe is only sensitive at high GO concentration. The interaction of GO with cell envelopes was also supported by the increased SS signal, which is related to cell complexity and cell volume. An increase in cell volume is probably due to alterations of the membrane permeability properties and failures in observed ($p < 0.01$) in FC assays (Fig. S3). *C. reinhardtii* cells exposed to 5 mg L^{-1}

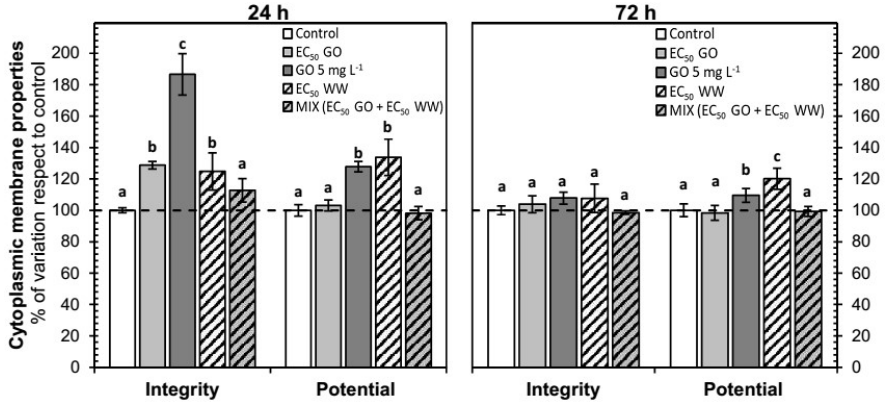

Figure 7. Alterations on cytoplasmic membrane properties of *C. reinhardtii* cells after 24 and 72 h of exposure. Results are shown as percentage of variation of membrane integrity and potential ± SD (n = 9) with respect to control (100% is indicated by the dashed line). Treatments with different letters are significantly different (Tukey's HSD, $p < 0.05$).

GO also showed a slight increase in the FS signal (Fig. S3), which could be attributed to a significant ($p < 0.001$) increase in the regulatory cell volume control process [40]. A previous study in *C. vulgaris* reported reduced cell permeability of the cytoplasmic membrane after exposure to GO for 96 h [41]. *C. reinhardtii* cells exposed to wastewater did exhibit a significant ($p < 0.01$) increase (+34 % for 24 h) of the $DiBAC_4(3)$ fluorescence emission. Membrane depolarisation coexisted with reduced membrane impairment, which can be attributed to plasma membrane damage occurring by permeation (increasing permeability) rather than membrane disruption [31, 42]. GO-wastewater mixtures induced the lowest PI and $DiBAC_4(3)$ fluorescence emissions, significantly lower than the GO (PI) or wastewater ($DiBAC_4(3)$) alone.

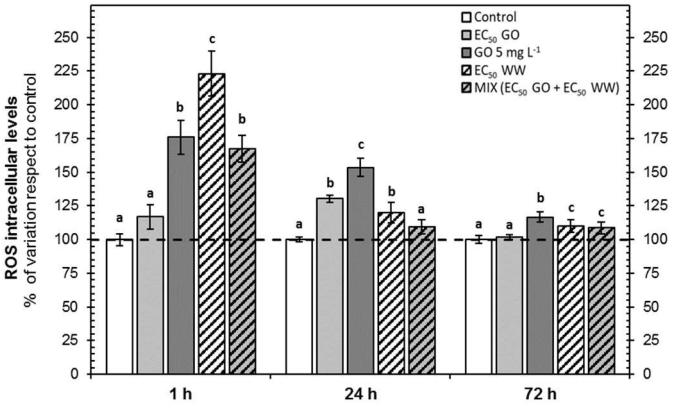

Figure 8. ROS intracellular levels of *C. reinhardtii* cells by FC using the fluorochrome H_2DCFDA after 1, 24 and 72 h of exposure. Results are shown as percentage of variation of ROS intracellular levels ± SD (n = 9) with respect to control (100% is indicated by the dashed line). Treatments with different letters are significantly different (Tukey's HSD, $p < 0.01$).

Oxidative stress has been proposed as the primary mechanism explaining the toxicity of GO and related materials [43, 44]. The production of intracellular ROS is shown in Fig. 8 as determined by general oxidative stress probe H_2DCFA after short (1 h) and long-term (24 and 72 h) exposures. Fig 8 shows that GO caused significant increase in ROS levels with maximum ROS formation after 24 h, which was reduced thereafter in agreement with the previously described findings about membrane integrity. An increase in ROS formation has also been reported in microalgae exposed to GO [45-47]. Hu *et al.*, showed that GO generated ROS are the probable cause of metabolic impairment in algal cells [48], but other researchers failed in finding ROS production and attributed the toxic effect to the depletion of the intracellular antioxidant glutathione [43]. The moderate levels of ROS production observed in this work were in agreement with data published elsewhere [44 35]. A significant feature observed in Fig. 8 is that the exposure of *C. reinhardtii* cells to wastewater strongly increased intracellular ROS levels. GO-wastewater mixtures, however resulted in less ROS formation than wastewater alone. Even after 24 h ROS formation in GO-wastewater mixture was significantly ($p < 0.001$) below the values observed in wastewater and GO individually. The oxidative effect of GO was also revealed by the membrane damage due to lipid oxidation, an effect that was reported before for graphene and carbon nanotubes [49, 50]. Fig. 9 shows that C4-BODIPY® fluorescence increased after GO exposure, indicating the presence of lipid peroxidation products. Upon exposure to wastewater, lipid peroxidation levels also increased, while GO-wastewater mixture treatment totally prevented lipid peroxidation. The results of lipid peroxidation followed the same pattern as ROS formation, clearly suggesting ROS formation-induced lipid peroxidation. The oxidation of polyunsaturated fatty acids could lead to the formation of pores and the increase of membrane permeability [51]. The overproduction of ROS could also explain the increase of intracellular complexity in cultures exposed to 5 mg L^{-1} of GO (Fig. S4), as a consequence of cell disorganisation.

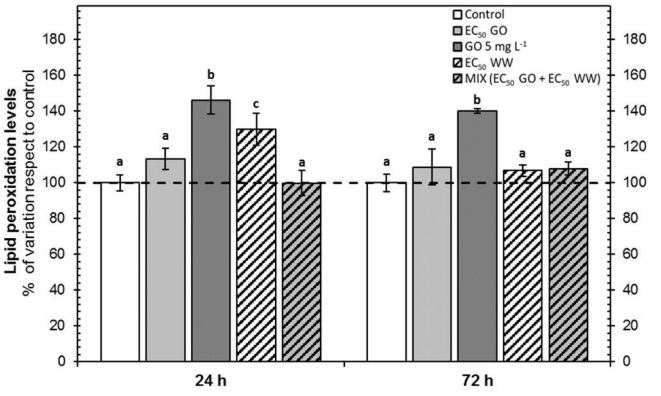

Figure 9. Lipid peroxidation levels of *C. reinhardtii* cells using FC and C4-Bodipy, after 24 and 72 h of exposure. Results are shown as percentage of variation of lipid peroxidation levels ± SD (n = 9) with respect to control (100% is indicated by the dashed line). Treatments with different letters are significantly different (Tukey's HSD, $p < 0.01$).

Intracellular free Ca^{2+}, $[Ca^{2+}]_c$, is an important second messenger in most cells and its regulation (homeostasis) is a key cellular parameter [34]. The changes in $[Ca^{2+}]_c$ induced by GO, wastewater and GO-wastewater mixtures were assessed after 1, 24 and 72 h of exposure of *C. reinhardtii* cells using Calcium Green-1 AM and FC. The results are shown in Fig. 10. After 1 h GO and wastewater induced significant elevation in $[Ca^{2+}]_c$ that decreased thereafter. The joint occurrence of cytoplasmic membrane depolarisation and the increase of cytosolic free calcium has been previously reported suggesting a possible interaction between these parameters [42]. As for the GO-wastewater mixtures, the elevation of $[Ca^{2+}]_c$ was lower than that of wastewater alone at the same dilution.

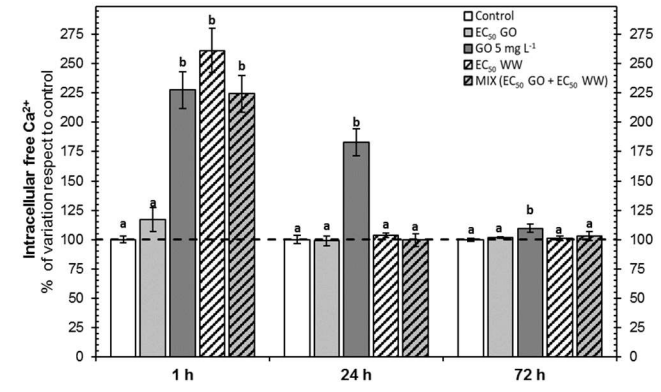

Figure 10. Intercellular free calcium, $[Ca^{2+}]_c$, for *C. reinhardtii* cells using FC and Calcium Green-1 AM after 1, 24 and 72 h of exposure. Results are shown as percentage of variation of intracellular free Ca^{2+} ± SD (n = 9) with respect to control (100% is indicated by the dashed line). Treatments with different letters are significantly different (Tukey's HSD, $p < 0.01$).

Mitochondria are important in the cellular response to environmental pollutants. The potential mitochondria membrane dysfunction induced by GO, wastewater and GO-wastewater binary combinations was assessed by FC using the fluorescent dye JC-1. The results, presented in Fig. 11, show that the ratio of orange/green fluorescence intensity significantly decreased after 24 h of exposure to GO, with an even greater decrease after 72 h, which indicated mitochondrial membrane depolarisation. Mitochondrial membrane potential loss is a common phenomenon in nanotoxicology [52, 53]. Oxidative stress is considered the primary reason for it [54, 55] and has been previously described for *C. vulgaris* exposed to GO [41, 45]. Fig. 11 also shows that wastewater exposure induced a dramatic mitochondrial membrane potential depolarisation in *C. reinhardtii* cells with reductions around 80 % with respect to controls ($p < 0.001$). Previous studies in *C. reinhardtii* cells have observed depolarisation of the mitochondrial membrane by chemical pollutants [34, 56]. The depolarisation of mitochondrial membrane can be attributed to a permeabilization of the inner membrane of the mitochondria as a consequence of lipid peroxidation due to ROS generation [57]. Our results showed the joint occurrence of significant depolarisation of the mitochondrial membrane (Fig. 11), an increase of lipid peroxidation (Fig. 9), and ROS formation (Fig. 8) in *C. reinhardtii* cells exposed to wastewater. Mitochondrial ROS formation was also studied using MitoTracker Orange CM-H2 TM ROS, a widely used ROS indicator (Fig. 11). GO exposure showed a significant enhancement of mitochondrial ROS, but the effect disappeared in GO-wastewater mixtures. In most mechanistic studies, the results showed that cells treated with the mixture GO-wastewater displayed similar level of damage than those exposed to GO or wastewater alone.

3.6. Ultrastructural observations

The ultrastructural alteration induced to *C. reinhardtii* by GO, wastewater and GO-wastewater mixtures after 72 h of exposure are shown in Fig. 12. Fig. 12A shows TEM images of non-exposed cells with intact ultrastructural morphology including cell wall, plasma membrane, chloroplast, nucleus and other cytoplasmic organelles. In non-exposed cells, the cell wall and plasma membrane are in tight contact, while plasmolysis is apparent with GO and wastewater exposure, as indicated by the double black arrows (Fig. 12 B and C). Other studies showed that GO induce plasmolysis in microalgae cells [41, 46].Together with plasmolysis, Fig. 12 B and C show an increased number of starch grains. The increase in the number of starch grains has been considered a self-defence mechanism induced by toxic agents in microalgae [58, 59]. Fig. 12 C and F show GO on the surface of the cells, while the damage to the cell wall is also observed in cells exposed to the GO-wastewater mixture (Fig. 12F). Hu *et al*. and Hazeem *et al*. showed GO covered cell surface in *C. vulgaris* and

GO forming a coating layer around *Pichoclorum* sp. cells, respectively [45, 60]. The oxygen and hydrogen containing groups on GO could favour the adhesion of GO onto cell surfaces through hydrogen bonds. Several authors proposed the internalization of GO through passive membrane penetration [41, 61]. TEM images of *C. reinhardtii* cells exposed to wastewater and GO-wastewater mixtures show shrinkage of the cytoplasm with irregular morphology of the plasma membrane and plasmolysis (Fig. 12 D, E and F).

3.7. Discussion on individual and mixture toxicity

The toxicity of graphene and GO materials has been attributed to several mechanisms. The direct contact with cell envelopes has been shown to produce damage to cell membranes. Graphene nanosheets have proven to be able to penetrate cell membranes and extract phospholipids from them as a consequence of the strong interactions between graphene and lipid molecules [62]. A work with a human hepatoma cell line demonstrated high affinity of GO for the plasma membrane, and the result was associated with membrane damage at concentrations in the few milligrams per litter range [63]. GO and cell membranes are both negatively charged under neutral or near neutral pH conditions. Therefore, a net electrostatic repulsion would be expected to keep GO apart from cells, which is the factor usually explaining why negatively charged particles are typically poorly internalized in cells [64]. However, neutral or negatively charged particles adsorb molecules from the environment either through electrostatic or hydrophobic interactions, which allow the nanoparticle to interface with the cell membrane [65]. It has been shown that increasing ionic strength also results in the reduction of electrostatic repulsion between GO and lipid bilayers [66]**.** Once attached, the process is essentially irreversible and deposited GO cannot be released from cell membranes even under ultrasonication, with the close interaction of GO and membranes being a necessary step for lipid membrane disruption [67]. Other authors have argued that the direct contact with GO sheets is not a requirement for bacterial inactivation [68]. The high free energy barrier for cell uptake faced by hydrophilic GO would make the direct interaction of cell membranes and GO a secondary mode of action with sporadic adhesion events likely due to cell lipopolysaccharide bridging.

Oxidative stress has been found to be a mechanism leading to the toxicity of GO to different cell lines by several experimental and theoretical studies [63, 69, 70]. The increase in intracellular ROS levels is accompanied by cellular ultrastructure alterations and changes in metabolic activity, including mitochondrial impairment [71]. However, the impact of GO on microorganisms is less clear with significant ROS levels observed at high exposure concentrations [44, 47]. Our results showed an increase in ROS formation, which, accompanied by lipid peroxidation, was unambiguously observed in cells exposed to GO. As a defence mechanism, *C. reinhardtii* cells exposed for 1 h to GO, displayed an increase in esterase activity and intracellular calcium levels. For more prolonged exposure to GO, the oxidative effect of ROS led to a decrease in the metabolic activity and the damage of cytoplasmic membrane. Our results suggest that the primary toxic pathway to *C. reinhardtii* would be oxidative, favoured by GO adsorption on cell envelopes and early revealed by membrane disruption. Besides oxidative damage to the cell membrane, GO

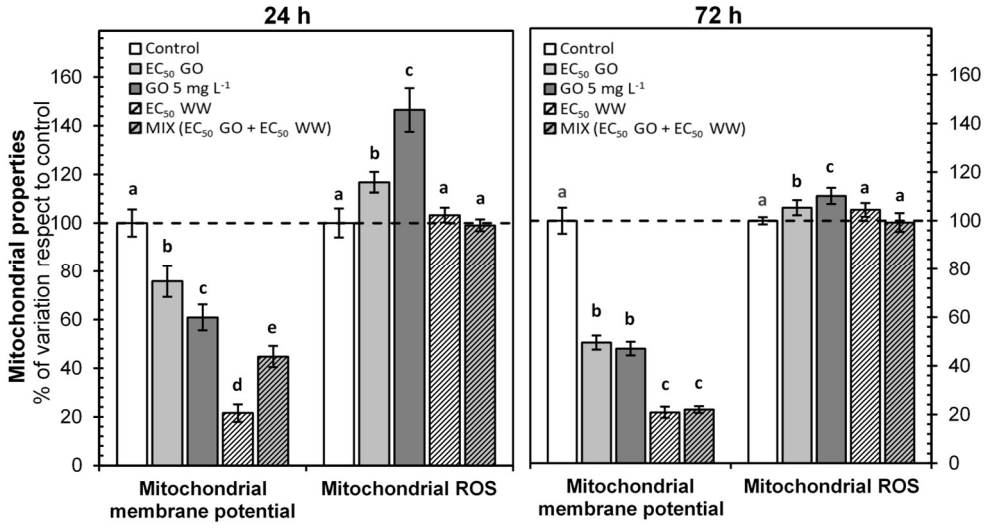

Figure 11. Alterations on mitochondrial properties of *C. reinhardtii* cells after 24 and 72 h of exposure. Results are shown as percentage of variation of mitochondrial membrane potential and mitochondrial ROS ± SD (n = 9) with respect to control (100% is indicated by the dashed line). Mitochondrial membrane potential changes were expressed as the mean orange (JC-1 oligomers) / green (JC-1 monomers) fluorescence intensity ratio. Treatments with different letters are significantly different (Tukey's HSD, $p < 0.001$).

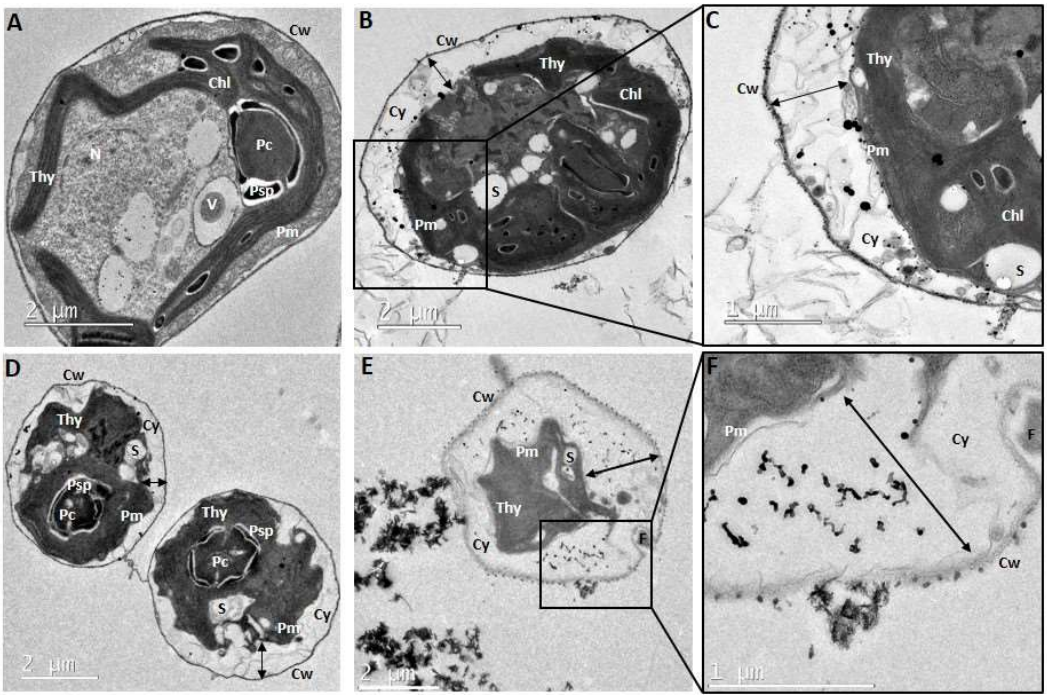

Figure 12. Representative TEM micrographs of *C. reinhardtii* (A) non-exposed and exposed to (B, C) 5 mg L^{-1} of GO, (D) 0.325 of wastewater effluent dilution, and (E, F) binary combination of GO and wastewater with a fixed ratio (EC_{50} GO + EC_{50} wastewater) for 72 h. Double black arrows indicate plasmolysis. Chl: chloroplast, Cw: cell wall, Cy: cytosol, F: flagella, N: nucleus, Pc: pyrenoid center, Pm: plasma membrane, Psp: pyrenoid starch plate, S: starch grain, Thy: thylakoid, V: vacuole.

exposure also resulted in mitochondrial ROS increase and a parallel decrease of mitochondrial membrane potential. Membrane damage and mitochondrial impairment were related to the increase in ROS levels, which was clearly observed in this work at intermediate (24 h) exposure times.

An important aspect of nanotoxicology is whether nanoparticles are internalized into the cell or not. Apart from the fact that negatively charged particles display weaker interactions with cells compared to those with positively charged surfaces, there are studies reporting clear evidences of GO internalization. GO nanoplatelets were shown to penetrate into the cytosol of human hepatocellular carcinoma cells where they concentrate enclosed in vesicles [63]. Specifically concerning algae, Hu et al. showed that GO with concentrations in the 0.1-10 mg L^{-1} range interacted with the surface of *C. vulgaris* cells and formed nanostructures with cell exudates. The authors claim that the observed plasmolysis and the increase in the number of starch grains were a consequence of GO internalization, but this possibility is controversial [32]. In this work, we did not find evidence of GO internalization in *C. reinhardtii* cells, but the results described above on the mechanisms of toxic action support the evidence found in TEM images about the interaction of GO with the surface of cells.

Wastewater led to a significant reduction of *C. reinhardtii* metabolic activity and membrane depolarisation because of a sharp and rapid production of ROS and an intense elevation of intracellular free calcium. The clear temporal differences in the toxic response to GO and wastewater, with rapid intracellular rupture of cell homeostasis and an absence of membrane impairment for the latter, were a consequence of the different mode of toxic action of nanoparticles and chemical pollutants. The absence of internalization and the indirect ROS formation after GO contact with cell envelopes explain the delayed toxicity observed with GO as compared to wastewater.

Although similar qualitatively, the effects caused by GO-wastewater binary combinations appeared significantly attenuated in cells exposed to mixtures. In all cases, we observed smaller increase in metabolic activity and reduced ROS production and intracellular free calcium levels than expected from the combination of GO and wastewater. Cytoplasmic membrane damage or the elevation of lipid peroxidation levels were not observed. These results supported the antagonistic effect observed by GO-wastewater mixture for the growth inhibition of *C. reinhardtii* cells.

To provide further insights on the reasons for the observed antagonism, the Isobolograms corresponding to two representative experiments are shown in Fig. 13. The two mixtures represented were taken from the experimental design of Fig. 1. and displayed affected fractions for growth inhibition in the $0.15 < f_a < 0.20$

range. One of the experiments, in blue, was performed using a non-constant ratio, while the other, in red, belongs to the constant ratio series of the experimental design. (The other non-constant ratio experiments with antagonistic mixtures are shown in Fig. S4, ESI). The lines in Fig. 13 represent additive mixtures at the same level of effect and correspond to the experimental point with the same colour. It is apparent that both experiments fall in the zone of antagonism and, in fact, their CI > 5.

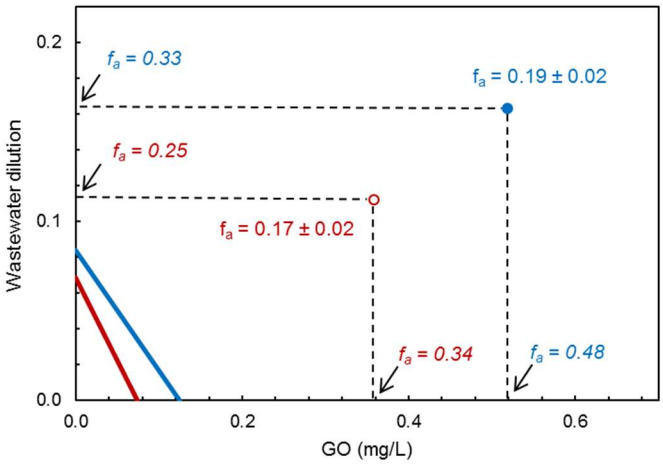

Figure 13. Isobolograms representing constant (○, red) and non-constant (●, blue) ratio binary combinations. Vertical distances represent wastewater dilution, and the lines correspond to predicted additivity at the same affected fraction values. Points with the same colour represent experimental toxicity with their corresponding errors.

The antagonistic effect of GO could be partially attributed to the adsorption of toxic chemicals on the surface of GO nanoparticles. The assumption is consistent with the absence of GO internalization and supported by the literature findings on the use of carbon nanomaterials for the sequestration of toxic compounds [72]. The adsorption capacity of GO for wastewater pollutants observed in this work is also in line with this hypothesis [13]. Considering the adsorption capacity of GO (for 10 mg L^{-1}) of 89.5 □g g^{-1}, as measured in this work, the amount of adsorbed compounds would represent > 30% of the total amount of the compounds quantified in wastewater at the dilution used for the experiments shown in Fig. 13. However, the results showed that the mere concentration of GO in GO-wastewater mixtures, would lead to individual toxicities (f_a) of 0.34 and 0.48 as indicated in the isobologram of Fig. 13.

Another possible explanation for the antagonistic toxic effects in the case of nanoparticle suspensions comes from the agglomeration or aggregation that nanoparticles undergo in contact with natural colloids. It has been described that GO aggregates in water depending on the presence of organic matter, particularly in the case of extracellular polymeric substances [73]. Accordingly, Table 1, shows that GO aggregated preferentially in wastewater with DLS particle size in the micron range after 24 h. The different size of aggregates is also observed in the TEM images of Fig. 12 and also in Fig. S5 (ESI) which compares two TEM images of *C. reinhardtii* cells exposed to GO in TP medium and in wastewater, clearly showing the larger aggregates formed in wastewater. The isobolograms also indicated that a reduction of GO availability as a consequence of particle aggregation does not completely explain the antagonistic effect observed in GO-wastewater mixtures. As shown in Fig. 13, wastewater in GO-wastewater mixtures would lead, acting singly, to considerably lower values of affected fraction with respect to those observed in mixtures. Similar arguments can be applied to other experiments as shown in Fig. S4 (ESI). The conclusion is that neither the adsorption of toxic compounds nor the reduced availability of GO due to aggregation in wastewater was enough to completely explain the observed antagonism, and a combination of both factors is probably the main reason for the results observed in this work. Another finding of this work is that non-additive behaviour was strongly concentration-dependent with antagonism observed only at low effect levels. The results show that it is premature to consider all possible non-additive interactions at low effect levels as negligible. The consequences are clear for regulatory frameworks for which any breaking of the additivity paradigm poses an important challenge.

4. Conclusions

This work reports the results of GO interaction with *C. reinhardtii* cells, the physical adsorption of the micropollutants from a treated wastewater and the toxicological interactions observed when algal cells were jointly exposed to GO and wastewater. The micropollutants quantified in wastewater were polar pharmaceuticals, metabolites and artificial sweeteners with concentrations ranging from the tens of ng L^{-1} to several □g L^{-1}. The total amount of compounds adsorbed on GO was 89.5 µg g^{-1} for GO 10 mg L^{-1}. The adsorption was higher for hydrophilic compounds.

GO impaired *C. reinhardtii* cells due to the oxidative damage of the cytoplasmic membrane. Short time defence responses consisted of an increase of intracellular calcium and metabolic activity. Long-term effect was associated with mitochondrial ROS formation with depolarisation of mitochondrial membrane. Wastewater induced rapid production of ROS and an intense elevation of intracellular free calcium. GO was not internalized; the toxicity being explained by ROS formation upon contact with cell envelopes.

The combination GO-wastewater displayed considerable antagonism for the lower values of the affected fraction. The antagonistic effect was attributed to the adsorption of toxic chemicals on the

surface of GO nanoparticles and to particle aggregation. The results show that non-additive toxicity of pollutant-nanoparticle mixtures exist and can be relevant for toxicity testing and regulatory frameworks.

Acknowledgements

Financial support was provided by the Spanish Ministry of Economy, CTM2016-74927-C2-1-R/2-R and the Dirección General de Universidades e Investigación de la Comunidad de Madrid, Network S2013/MAE-2716. Idoia Martín-de-Lucía thanks the Spanish Ministry of Economy for the award of a FPI contract (BES-2014-070093)

References

1. R. Rosal, A. Rodríguez, J. A. Perdigón-Melón, A. Petre, E. García-Calvo, M. J. Gómez, A. Agüera and A. R. Fernández-Alba, Occurrence of emerging pollutants in urban wastewater and their removal through biological treatment followed by ozonation, *Water Research*, 2010, **44**, 578-588.
2. B. Petrie, R. Barden and B. Kasprzyk-Hordern, A review on emerging contaminants in wastewaters and the environment: Current knowledge, understudied areas and recommendations for future monitoring, *Water Research*, 2015, **72**, 3-27.
3. C. Aristizabal-Ciro, A. M. Botero-Coy, F. J. López and G. A. Peñuela, Monitoring pharmaceuticals and personal care products in reservoir water used for drinking water supply, *Environmental Science and Pollution Research*, 2017, **24**, 7335-7347.
4. A. Jelić, M. Gros, M. Petrović, A. Ginebreda and D. Barceló, in *Emerging and Priority Pollutants in Rivers: Bringing Science into River Management Plans*, eds. H. Guasch, A. Ginebreda and A. Geiszinger, Springer Berlin Heidelberg, Berlin, Heidelberg, 2012, DOI: 10.1007/978-3-642-25722-3_1, pp. 1-23.
5. A. A. Godoy and F. Kummrow, What do we know about the ecotoxicology of pharmaceutical and personal care product mixtures? A critical review, *Critical Reviews in Environmental Science and Technology*, 2017, **47**, 1453-1496.
6. E. Commission, *Toxicity and Assessment of Chemical Mixtures*, Scientific Committee on Health and Environmental Risks (SCHER), Scientific Committee on Emerging and Newly Identified Health Risks (SCENIHR) and Scientific Committee on Consumer Safety (SCCS), Brussels, 2012.
7. C. Marx, V. Mühlbauer, P. Krebs and V. Kuehn, Environmental risk assessment of antibiotics including synergistic and antagonistic combination effects, *Science of The Total Environment*, 2015, **524**, 269-279.
8. T. Backhaus, Environmental risk assessment of pharmaceutical mixtures: Demands, gaps, and possible bridges, *The AAPS Journal*, 2016, **18**, 804-813.
9. S. K. Brar, M. Verma, R. D. Tyagi and R. Y. Surampalli, Engineered nanoparticles in wastewater and wastewater sludge – Evidence and impacts, *Waste Management*, 2010, **30**, 504-520.
10. J. R. Lead and K. J. Wilkinson, Aquatic colloids and nanoparticles: Current knowledge and future trends, *Environmental Chemistry*, 2006, **3**, 159-171.
11. I. Lynch and K. A. Dawson, Protein-nanoparticle interactions, *Nano Today*, 2008, **3**, 40-47.
12. I. Martin-de-Lucia, M. C. Campos-Manas, A. Aguera, I. Rodea-Palomares, G. Pulido-Reyes, F. Leganes, F. Fernandez-Pinas and R. Rosal, Reverse Trojan-horse effect decreased wastewater toxicity in the presence of inorganic nanoparticles, *Environmental Science: Nano*, 2017, **4**, 1273-1282.
13. J. L. Falconer, C. F. Jones, S. Lu and D. W. Grainger, Carbon nanomaterials rescue phenanthrene toxicity in zebrafish embryo cultures, *Environmental Science: Nano*, 2015, **2**, 645-652.
14. J. Sanchís, M. Olmos, P. Vincent, M. Farré and D. Barceló, New insights on the influence of organic co-contaminants on the aquatic toxicology of carbon nanomaterials, *Environmental Science & Technology*, 2015, **50**, 961-969.
15. D. R. Dreyer, S. Park, C. W. Bielawski and R. S. Ruoff, The chemistry of graphene oxide, *Chemical Society Reviews*, 2010, **39**, 228-240.
16. O. Akhavan and E. Ghaderi, Toxicity of graphene and graphene oxide nanowalls against bacteria, *ACS Nano*, 2010, **4**, 5731-5736.
17. S. Romero-Vargas, F. Perreault, A. F. de Faria and M. Elimelech, Interaction of graphene oxide with bacterial cell membranes: Insights from force spectroscopy, *Environmental Science & Technology Letters*, 2015, **2**, 112-117.
18. T. C. Chou and P. Talalay, Quantitative analysis of dose-effect relationships: the combined effects of multiple drugs or enzyme inhibitors, *Advances in Enzyme Regulation*, 1984, **22**, 27-55.
19. M. C. Campos-Mañas, P. Plaza-Bolaños, J. A. Sánchez-Pérez, S. Malato and A. Agüera, Fast determination of pesticides and other contaminants of emerging concern in treated wastewater using direct injection coupled to highly sensitive ultra-high performance liquid chromatography-tandem mass spectrometry, *Journal of Chromatography A*, 2017, **1507**, 84-94.
20. E. H. Harris, in *The Chlamydomonas Sourcebook*, Academic Press, San Diego, 1989,

DOI: https://doi.org/10.1016/B978-0-12-326880-8.50004-3, p. xi.
21. C. Ritz, F. Baty, J. C. Streibig and D. Gerhard, Dose-tesponse analysis using R, *PLOS ONE*, 2016, **10**, e0146021.
22. C. Ritz and J. C. Streibig, Bioassay analysis using R, *Journal of Statistical Software*, 2005, **012**.
23. T. C. Chou, Theoretical basis, experimental design, and computerized simulation of synergism and antagonism in drug combination studies, *Pharmacological Reviews*, 2006, **58**, 621-681.
24. T. C. Chou and N. Martin, *CompuSyn for Drug Combinations and for General Dose-Effect Analysis, Software and User's Guide: A Computer Program for Quantitation of Synergism and Antagonism in Drug Combinations, and the Determination of IC50 and ED50 and LD50 Values*, ComboSyn Inc, Paramus, NJ, USA, 2005.
25. R. Prado, R. García, C. Rioboo, C. Herrero, J. Abalde and A. Cid, Comparison of the sensitivity of different toxicity test endpoints in a microalga exposed to the herbicide paraquat, *Environment International*, 2009, **35**, 240-247.
26. C. Wolff, B. Fuks and P. Chatelain, Comparative study of membrane potential-sensitive fluorescent probes and their use in ion channel screening assays, *Journal of Biomolecular Screening*, 2003, **8**, 533-543.
27. J. Fox, Getting started with the R commander: a basic-statistics graphical user interface to R, *Journal of Statistical Software*, 2005, **14**, 1-42.
28. A. Imai, T. Fukushima, K. Matsushige, Y. H. Kim and K. Choi, Characterization of dissolved organic matter in effluents from wastewater treatment plants, *Water Research*, 2002, **36**, 859-870.
29. O. C. Compton and S. T. Nguyen, Graphene oxide, highly reduced graphene oxide, and graphene: Versatile building blocks for carbon-based materials, *Small*, 2010, **6**, 711-723.
30. X. Sanchez-Vila, E. Vàzquez-Suñé, P. Rodríguez-Escales, A. Jurado, A. Folch, A. Carles-Brangarí, J. Carrera and D. Fernàndez-Garcia, in *Emerging Contaminants in River Ecosystems: Occurrence and Effects Under Multiple Stress Conditions*, eds. M. Petrovic, S. Sabater, A. Elosegi and D. Barceló, Springer International Publishing, Cham, 2016, DOI: 10.1007/698_2015_5010, pp. 47-75.
31. M. Seoane, M. Esperanza, C. Rioboo, C. Herrero and Á. Cid, Flow cytometric assay to assess short-term effects of personal care products on the marine microalga *Tetraselmis suecica*, *Chemosphere*, 2017, **171**, 339-347.
32. X. Hu, K. Lu, L. Mu, J. Kang and Q. Zhou, Interactions between graphene oxide and plant cells: Regulation of cell morphology, uptake, organelle damage, oxidative effects and metabolic disorders, *Carbon*, 2014, **80**, 665-676.
33. M. Esperanza, M. Seoane, C. Rioboo, C. Herrero and Á. Cid, Chlamydomonas reinhardtii cells adjust the metabolism to maintain viability in response to atrazine stress, *Aquatic Toxicology*, 2015, **165**, 64-72.
34. M. González-Pleiter, C. Rioboo, M. Reguera, I. Abreu, F. Leganés, Á. Cid and F. Fernández-Piñas, Calcium mediates the cellular response of *Chlamydomonas reinhardtii* to the emerging aquatic pollutant triclosan, *Aquatic Toxicology*, 2017, **186**, 50-66.
35. P. F. M. Nogueira, D. Nakabayashi and V. Zucolotto, The effects of graphene oxide on green algae *Raphidocelis subcapitata*, *Aquatic Toxicology*, 2015, **166**, 29-35.
36. K. Wang, J. Ruan, H. Song, J. Zhang, Y. Wo, S. Guo and D. Cui, Biocompatibility of graphene oxide, *Nanoscale Research Letters*, 2011, **6**, 8-8.
37. L. Wei, M. Thakkar, Y. Chen, S. A. Ntim, S. Mitra and X. Zhang, Cytotoxicity effects of water dispersible oxidized multiwalled carbon nanotubes on marine alga *Dunaliella tertiolecta*, *Aquatic Toxicology*, 2010, **100**, 194-201.
38. Y. Tang, J. Tian, S. Li, C. Xue, Z. Xue, D. Yin and S. Yu, Combined effects of graphene oxide and Cd on the photosynthetic capacity and survival of *Microcystis aeruginosa*, *Science of The Total Environment*, 2015, **532**, 154-161.
39. P. Tsiaka, V. Tsarpali, I. Ntaikou, M. N. Kostopoulou, G. Lyberatos and S. Dailianis, Carbamazepine-mediated pro-oxidant effects on the unicellular marine algal species *Dunaliella tertiolecta* and the hemocytes of mussel *Mytilus galloprovincialis*, *Ecotoxicology*, 2013, **22**, 1208-1220.
40. H. U. Riisgård, K. Nørgård Nielsen and B. Søgaard-Jensen, Further studies on volume regulation and effects of copper in relation to pH and EDTA in the naked marine flagellate *Dunaliella marina*, *Marine Biology*, 1980, **56**, 267-276.
41. S. Ouyang, X. Hu and Q. Zhou, Envelopment–internalization synergistic effects and metabolic mechanisms of graphene oxide on single-cell *Chlorella vulgaris* Are dependent on the nanomaterial particle size, *ACS Applied Materials & Interfaces*, 2015, **7**, 18104-18112.
42. R. Prado, C. Rioboo, C. Herrero and Á. Cid, Screening acute cytotoxicity biomarkers using a microalga as test organism, *Ecotoxicology and Environmental Safety*, 2012, **86**, 219-226.
43. F. Perreault, A. F. de Faria, S. Nejati and M. Elimelech, Antimicrobial properties of graphene oxide nanosheets: Why size matters, *ACS Nano*, 2015, **9**, 7226-7236.

44. Z. Guo, C. Xie, P. Zhang, J. Zhang, G. Wang, X. He, Y. Ma, B. Zhao and Z. Zhang, Toxicity and transformation of graphene oxide and reduced graphene oxide in bacteria biofilm, *Science of The Total Environment*, 2017, **580**, 1300-1308.
45. X. Hu, S. Ouyang, L. Mu, J. An and Q. Zhou, Effects of graphene oxide and oxidized carbon nanotubes on the cellular division, microstructure, uptake, oxidative stress, and metabolic profiles, *Environmental Science & Technology*, 2015, **49**, 10825-10833.
46. X. Hu, Y. Gao and Z. Fang, Integrating metabolic analysis with biological endpoints provides insight into nanotoxicological mechanisms of graphene oxide: From effect onset to cessation, *Carbon*, 2016, **109**, 65-73.
47. J. Zhao, X. Cao, Z. Wang, Y. Dai and B. Xing, Mechanistic understanding toward the toxicity of graphene-family materials to freshwater algae, *Water Research*, 2017, **111**, 18-27.
48. C. Hu, N. Hu, X. Li and Y. Zhao, Graphene oxide alleviates the ecotoxicity of copper on the freshwater microalga *Scenedesmus obliquus*, *Ecotoxicology and Environmental Safety*, 2016, **132**, 360-365.
49. K. Krishnamoorthy, M. Veerapandian, L. H. Zhang, K. Yun and S. J. Kim, Antibacterial efficiency of graphene nanosheets against pathogenic bacteria via lipid peroxidation, *The Journal of Physical Chemistry C*, 2012, **116**, 17280-17287.
50. C. D. Vecitis, K. R. Zodrow, S. Kang and M. Elimelech, Electronic-structure-dependent bacterial cytotoxicity of single-walled carbon nanotubes, *ACS Nano*, 2010, **4**, 5471-5479.
51. J. Van der Paal, E. C. Neyts, C. C. W. Verlackt and A. Bogaerts, Effect of lipid peroxidation on membrane permeability of cancer and normal cells subjected to oxidative stress, *Chemical Science*, 2016, **7**, 489-498.
52. S. Höss, A. Fritzsche, C. Meyer, J. Bosch, R. U. Meckenstock and K. U. Totsche, Size- and composition-dependent toxicity of synthetic and soil-derived Fe oxide colloids for the nematode *Caenorhabditis elegans*, *Environmental Science & Technology*, 2015, **49**, 544-552.
53. C. Filippi, A. Pryde, P. Cowan, T. Lee, P. Hayes, K. Donaldson, J. Plevris and V. Stone, Toxicology of ZnO and TiO_2 nanoparticles on hepatocytes: Impact on metabolism and bioenergetics, *Nanotoxicology*, 2015, **9**, 126-134.
54. A. V. Singh, K. K. Mehta, K. Worley, J. S. Dordick, R. S. Kane and L. Q. Wan, Carbon nanotube-induced loss of multicellular chirality on micropatterned substrate is mediated by oxidative stress, *ACS Nano*, 2014, **8**, 2196-2205.
55. Y. H. Lee, F. Y. Cheng, H. W. Chiu, J. C. Tsai, C. Y. Fang, C. W. Chen and Y. J. Wang, Cytotoxicity, oxidative stress, apoptosis and the autophagic effects of silver nanoparticles in mouse embryonic fibroblasts, *Biomaterials*, 2014, **35**, 4706-4715.
56. M. Esperanza, A. Cid, C. Herrero and C. Rioboo, Acute effects of a prooxidant herbicide on the microalga *Chlamydomonas reinhardtii*: Screening cytotoxicity and genotoxicity endpoints, *Aquatic Toxicology*, 2015, **165**, 210-221.
57. C. M. Palmeira, A. J. Moreno and V. M. C. Madeira, Mitochondrial bioenergetics is affected by the herbicide paraquat, *Biochimica et Biophysica Acta (BBA) - Bioenergetics*, 1995, **1229**, 187-192.
58. C. Luo, Y. Li, L. Yang, X. Wang, J. Long and J. Liu, Superparamagnetic iron oxide nanoparticles exacerbate the risks of reactive oxygen species-mediated external stresses, *Archives of Toxicology*, 2015, **89**, 357-369.
59. H. S. Jiang, X. N. Qiu, G. B. Li, W. Li and L. Y. Yin, Silver nanoparticles induced accumulation of reactive oxygen species and alteration of antioxidant systems in the aquatic plant *Spirodela polyrhiza*, *Environmental Toxicology and Chemistry*, 2014, **33**, 1398-1405.
60. L. J. Hazeem, M. Bououdina, E. Dewailly, C. Slomianny, A. Barras, Y. Coffinier, S. Szunerits and R. Boukherroub, Toxicity effect of graphene oxide on growth and photosynthetic pigment of the marine alga *Picochlorum* sp. during different growth stages, *Environmental Science and Pollution Research*, 2017, **24**, 4144-4152.
61. Y. Li, H. Yuan, A. von dem Bussche, M. Creighton, R. H. Hurt, A. B. Kane and H. Gao, Graphene microsheets enter cells through spontaneous membrane penetration at edge asperities and corner sites, *Proceedings of the National Academy of Sciences*, 2013, **110**, 12295-12300.
62. Y. Tu, M. Lv, P. Xiu, T. Huynh, M. Zhang, M. Castelli, Z. Liu, Q. Huang, C. Fan, H. Fang and R. Zhou, Destructive extraction of phospholipids from Escherichia coli membranes by graphene nanosheets, 2013, **8**, 968.
63. T. Lammel, P. Boisseaux, M. L. Fernández-Cruz and J. M. Navas, Internalization and cytotoxicity of graphene oxide and carboxyl graphene nanoplatelets in the human hepatocellular carcinoma cell line Hep G2, *Particle and Fibre Toxicology*, 2013, **10**, 27.
64. A. Verma and F. Stellacci, Effect of surface properties on nanoparticle–cell interactions, *Small*, 2010, **6**, 12-21.
65. V. Forest and J. Pourchez, Preferential binding of positive nanoparticles on cell membranes is due to electrostatic interactions: A too simplistic explanation that does not take into account the nanoparticle protein corona, *Materials Science and Engineering: C*, 2017, **70**, 889-896.

66. X. Liu and K. L. Chen, Interactions of graphene oxide with model cell membranes: Probing nanoparticle attachment and lipid bilayer disruption, *Langmuir*, 2015, **31**, 12076-12086.
67. S. Liu, M. Hu, T. H. Zeng, R. Wu, R. Jiang, J. Wei, L. Wang, J. Kong and Y. Chen, Lateral dimension-dependent antibacterial activity of graphene oxide sheets, *Langmuir*, 2012, **28**, 12364-12372.
68. J. D. Mangadlao, C. M. Santos, M. J. L. Felipe, A. C. C. de Leon, D. F. Rodrigues and R. C. Advincula, On the antibacterial mechanism of graphene oxide (GO) Langmuir-Blodgett films, *Chemical Communications*, 2015, **51**, 2886-2889.
69. A. M. Pinto, I. C. Gonçalves and F. D. Magalhães, Graphene-based materials biocompatibility: A review, *Colloids and Surfaces B: Biointerfaces*, 2013, **111**, 188-202.
70. M. Golkaram and A. C. T. van Duin, Revealing graphene oxide toxicity mechanisms: A reactive molecular dynamics study, *Materials Discovery*, 2015, **1**, 54-62.
71. K. Yang, Y. Li, X. Tan, R. Peng and Z. Liu, Behavior and toxicity of graphene and Its functionalized derivatives in biological systems, *Small*, 2013, **9**, 1492-1503.
72. E. J. Petersen, R. A. Pinto, P. F. Landrum and W. J. Weber, Influence of carbon nanotubes on pyrene bioaccumulation from contaminated soils by earthworms, *Environmental Science & Technology*, 2009, **43**, 4181-4187.
73. M. A. Maurer-Jones, I. L. Gunsolus, C. J. Murphy and C. L. Haynes, Toxicity of engineered nanoparticles in the environment, *Analytical Chemistry*, 2013, **85**, 3036-3049.

Electronic Supplementary Information

Combined toxicity of graphene oxide and wastewater to the green alga *Chlamydomonas reinhardtii*

Idoia Martín-de-Lucía[1], Marina C. Campos-Mañas[2] Ana Agüera[2], Francisco Leganés[3], Francisca Fernández-Piñas[3], Roberto Rosal[1,*]

[1] Department of Chemical Engineering, University of Alcalá, E-28871 Alcalá de Henares, Madrid, Spain
[2] CIESOL, Joint Centre of the University of Almería-CIEMAT, La Cañada de San Urbano, 04120 Almería, Spain
[3] Department of Biology, Faculty of Science, Universidad Autónoma de Madrid, E-28049, Spain

* corresponding author: roberto.rosal@uah.es

CONTENTS:

Table S1. Wastewater characterization parameters (0.45 μm filtered samples).

Parameters	**value**	**Ions**	**(mg/L)**
pH	6.5*	Nitrate	0.38
Turbidity (NTU)	1.4	Chloride	125.5
Conductivity (mS/cm)	1.23 ± 0.03	Sulphate	143.7
COD (mg/L)	49.2 ± 1.2	Fluoride	<0.80
NPOC (mg/L)	17.2 ± 0.5	Nitrite	<0.10
Suspended solids (mg/L)	7.6	Bicarbonate	348.4
Alkalinity (mg $CaCO_3$/L)	286		
Total-P (mg/L)	0.1	Sodium	95.3
Total-N (mg/L)	2.3	Potassium	23.4
		Magnesium	14.3
		Calcium	49
		Ammonium	68.4

* Measured just before runs.

Table S2. Experimental design for determining toxicological interactions of GO and wastewater (WW) and their binary combinations for *C. reinhardtii* growth inhibition.

Constant ratio			**Non-constant ratio**			
Dilutions	Binary combinations GO+WW (1:0.3)		Dilutions GO	Dilutions WW	Binary combinations GO+WW ($WW = -0.3\,GO + 0.3$)	
	GO (mg L^{-1})	WW (dil.)			GO (mg L^{-1})	WW (dil.)
$\frac{1}{2.9}$ (EC_{50})	0.36	0.11	$\frac{1}{1.2}$ (EC_{50})	$\frac{1}{6}$ (EC_{50})	0.86	0.05
$\frac{1}{1.7}$ (EC_{50})	0.61	0.19	$\frac{1}{1.5}$ (EC_{50})	$\frac{1}{3}$ (EC_{50})	0.69	0.11
1 (EC_{50})	1.04	0.33	$\frac{1}{2}$ (EC_{50})	$\frac{1}{2}$ (EC_{50})	0.52	0.16
1.7 (EC_{50})	1.76	0.55	$\frac{1}{3}$ (EC_{50})	$\frac{1}{1.5}$ (EC_{50})	0.35	0.22
2.9 (EC_{50})	2.99	0.94	$\frac{1}{6}$ (EC_{50})	$\frac{1}{1.2}$ (EC_{50})	0.17	0.27

Table S3. Concentrations and physicochemical properties of pollutants detected in wastewater.

No.	Compound	Concentration (ng/L)	CAS Number	Molecular formula	log K_{ow}	pK_a	Acid/Base	log D_{ow} (pH 6.5)	Charge (+/-)	Main use
1	4-FAA*	6597 ± 326	1672-58-8	$C_{12}H_{13}N_3O_2$	-0.41	5.0	Weakly basic	-0.42	0.0	Metabolite of aminopyrine
2	Acesulfame	110 ± 2	33665-90-6	$C_4H_5NO_4S$	-1.33	5.7	Acidic	-1.39	-1.0	Sweetener
3	Amitriptyline	56 ± 9	50-48-6	$C_{20}H_{23}N$	4.92	9.4	Basic	2.00	1.0	Antidepressant
4	Antipyrine	2690 ± 337	60-80-0	$C_{11}H_{12}N_2O$	0.38	1.4	Weakly basic	0.38	0.0	Analgesic
5	Azithromycin	206 ± 9.4	83905-01-5	$C_{38}H_{72}N_2O_{12}$	4.02	8.7	Basic	1.76	1.0	Antibiotic
6	Bezafibrate	140 ± 12	41859-67-0	$C_{19}H_{20}ClNO_4$	4.25	3.61	Acidic	1.38	-1.0	Antilipemic
7	Carbamazepine	297 ± 5.1	298-46-4	$C_{15}H_{12}N_2O$	2.45		Neutral	2.45	0.0	Antiepileptic
8	Carbamazepine epoxide	67 ± 1	36507-30-9	$C_{15}H_{12}N_2O_2$	1.58		Neutral	1.58	0.0	Metabolite of carbamazepine
9	Ciprofloxacin	177 ± 34	85721-33-1	$C_{17}H_{18}FN_3O_3$	0.28	6.1/8.7	Zwitterionic	n.a.	-1.0	Antibiotic
10	Citalopram	214 ± 2.4	59729-33-8	$C_{20}H_{21}FN_2O$	3.74	9.7	Basic	0.52	1.0	Antidepressant
11	Clarithromycin	164 ± 25	81103-11-9	$C_{38}H_{69}NO_{13}$	3.16	9.0	Basic	0.65	1.0	Antibiotic
12	Diazepam	24 ± 2	439-14-5	$C_{16}H_{13}ClN_2O$	2.82	3.4	Weakly basic	2.82	0.0	Anxiolytic
13	Erythromycin	134 ± 2	114-07-8	$C_{37}H_{67}NO_{13}$	3.06	8.9	Basic	0.64	1.0	Antibiotic
14	Fenofibric acid	172 ± 7	42017-89-0	$C_{17}H_{15}ClNO_4$	4.00	3.1	Acidic	0.62	-1.0	Metabolite of fenofibrate
15	Furosemide	984 ± 30	54-31-9	$C_{12}H_{11}ClN_2O_5S$	2.03	3.8	Acidic	-0.65	-1.0	Antihypertensive
16	Gemfibrozil	2522 ± 49	25812-30-0	$C_{15}H_{22}O_3$	4.77	4.5	Acidic	2.79	-1.00	Antilipemic
17	Hydrochlorothiazide	2510 ± 85	58-93-5	$C_7H_8ClN_3O_4S_2$	-0.07	7.9/9.2	Basic	-4.23	1.00	Antihypertensive
18	Indomethacin	26 ± 5	53-86-1	$C_{19}H_{16}ClNO_4$	4.27	4.5	Acidic	2.29	-1.00	Analgesic
19	Lidocaine	447 ± 64	137-58-6	$C_{14}H_{22}N_2O$	2.44	7.8	Basic	1.15	1.00	Anesthetic

Table S3 (cont.). Concentrations and physicochemical properties of pollutants contained in wastewater.

No.	Compound	Concentration (ng/L)	CAS Number	Molecular formula	log K_{ow}	pK_a	Acid/Base	log D_{ow}**	Charge (+/-)	Main use
20	Mepivacaine	40 ± 4	96-88-8	$C_{15}H_{22}N_{20}$	1.95	7.7	Basic	0.70	1.00	Anesthetic
21	Metoclopramide	49 ± 2	364-62-5	$C_{14}H_{22}ClN_3O_2$	2.62	9.3	Basic	-0.17	1.00	Antiemetic
22	Metoprolol	38 ± 2	37350-58-6	$C_{15}H_{25}NO_3$	1.88	9.7	Basic	-1.34	1.00	β-blocker
23	Ofloxacin	472 ± 39	82419-36-1	$C_{18}H_{20}FN_3O_4$	-0.39	6.1/8.2	Zwitterionic	n.a.	-1.0	Antibiotic
24	Paraxanthine	251 ± 36	611-59-6	$C_7H_8N_4O_2$	-0.22	10.8	Weakly basic	-0.22	0.00	Metabolite of caffeine
25	Pentoxifylline	275 ± 20	06/05/6493	$C_{13}H_{18}N_4O_3$	0.29	0.3	Basic	0.29	0.00	Vasodilator
26	Primidone	370 ± 3	125-33-7	$C_{12}H_{14}N_2O_2$	0.91	12.3	Weak acid	0.91	0.00	Antiepileptic
27	Ranitidine	857 ± 43	66357-35-5	$C_{13}H_{22}N_4O_3S$	0.27	2.3/8.2	Diprotic base	-1.46	1.00	Antiacid
28	Sucralose	2117 ± 157	56038-13-2	$C_{12}H_{19}Cl3O_8$	-1.00	11.8	Neutral	11.8	0.0	Sweetener
29	Sulfamethoxazole	576 ± 15	723-46-6	$C_{10}H_{11}N_3O_3S$	0.89	1.8/5.6	Amphiprotic	-0.04	-1.0	Antibiotic
30	Sulfapyridine	313 ± 34	144-83-2	$C_{11}H_{11}N_3O_2S$	0.35	2.3/8.4	Amphiprotic	0.35	-1.0	Antibiotic
31	Theophylline	235 ± 31	58-55-9	$C_7H_8N_4O_2$	-0.02	8.8	Basic	-2.35	1.0	Bronchodilator/ Vasodilator
32	Trimethoprim	602 ± 21	738-70-5	$C_{14}H_{18}N_4O_2$	0.91	7.1	Basic	0.20	1.0	Antibiotic
33	Venlafaxine	559 ± 51	93413-69-5	$C_{17}H_{27}NO_2$	3.20	9.4	Basic	0.28	1.0	Antidepressant

* NFAA = N-formyl-4-aminoantipyrine
** pH 6.5

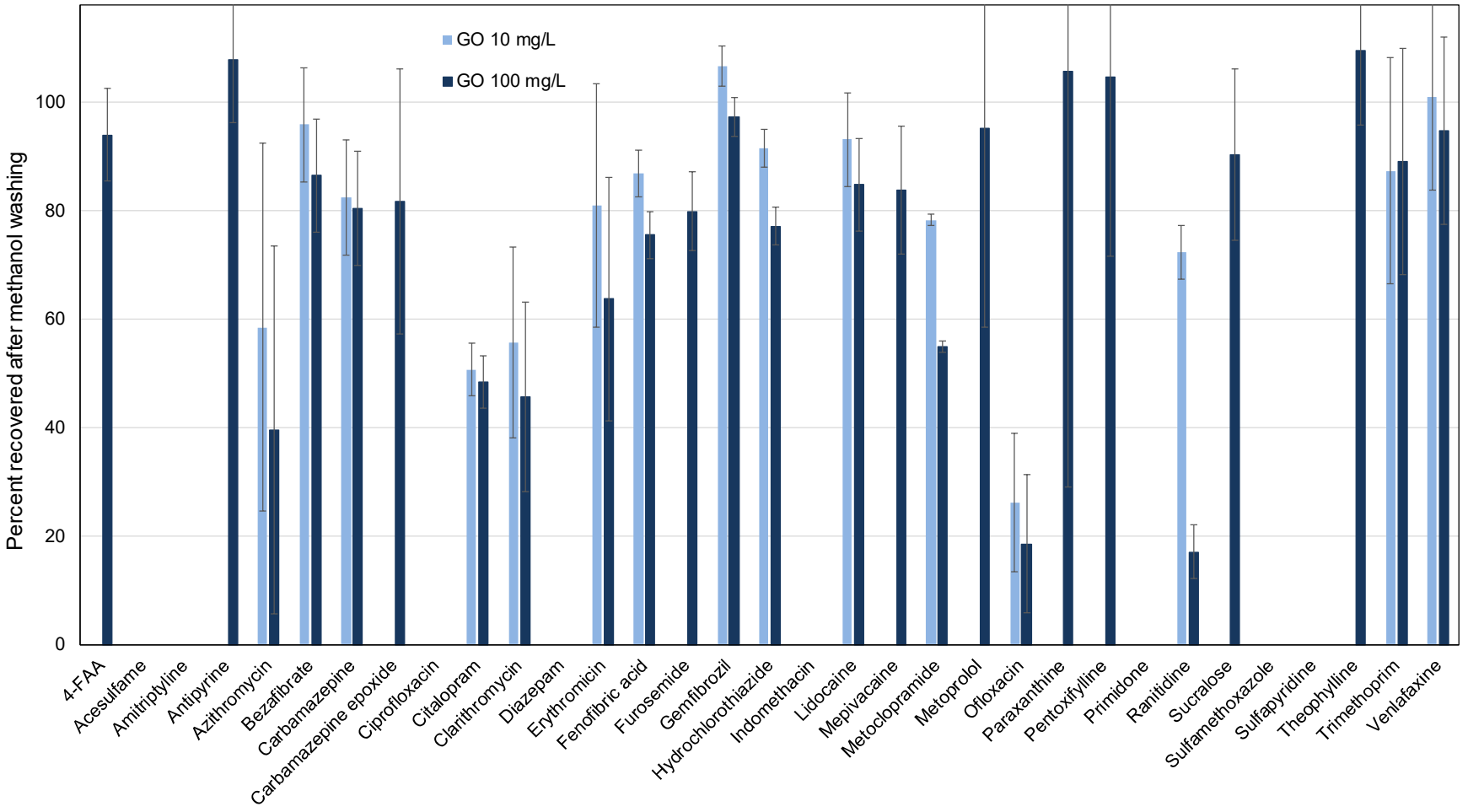

Figure S1. Percent recovery of wastewater pollutants after washing twice with methanol. (The results are shown only for compounds significantly adsorbed on GO nanoparticles; error bars represent standard deviation.)

a)

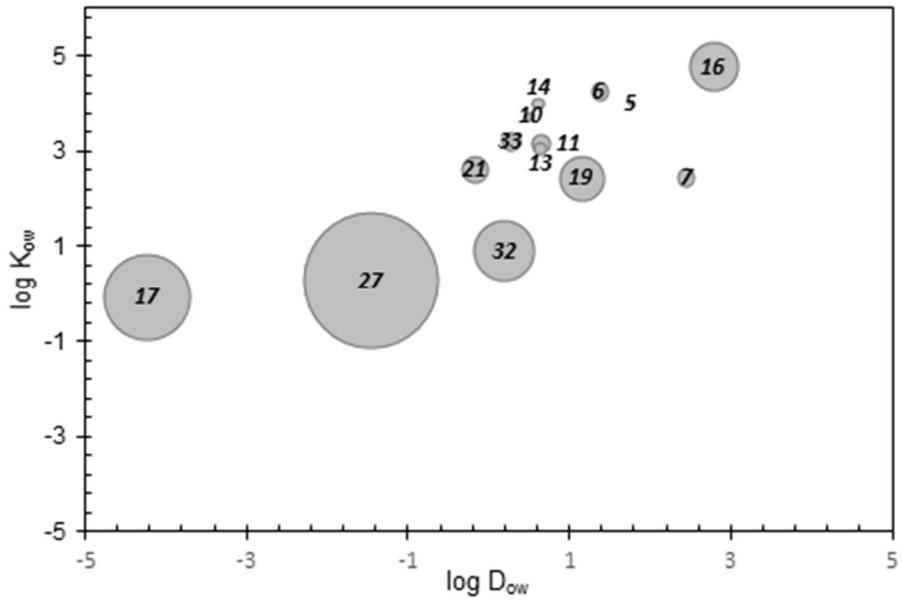

b)

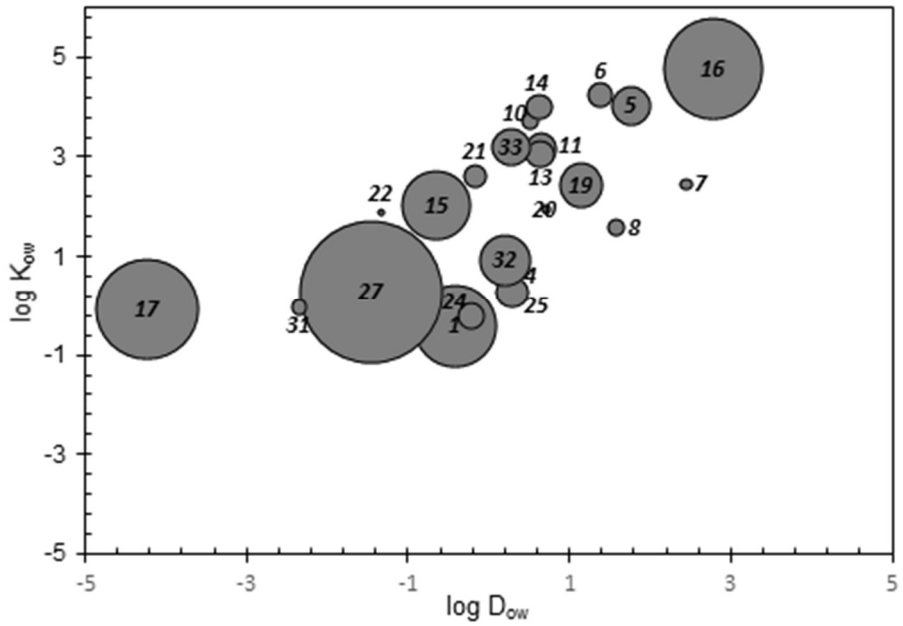

Figure S2. Amount adsorbed (size of bubble proportional to the amount adsorbed in μg/g) as a function of D_{ow}, and K_{ow} (Table S3). The results are shown for compounds significantly adsorbed with respect to the experimental error. Compounds numbered as in Table S3. (a) 10 mg L^{-1} GO, (b) 100 mg L^{-1} GO.

Table S4. Dose-effect parameters for the growth inhibition of *C. reinhardtii* after 72 h of exposure.

	GO (mg L^{-1})				WW (effluent dilution)			
	EC_x	**SD**	**CI_L 95%**	**CI_L 95%**	**EC_x**	**SD**	**CI_L 95%**	**CI_L 95%**
EC_{20}	0.035	0.004	0.027	0.042	0.109	0.006	0.097	0.121
EC_{50}	1.036	0.055	0.926	1.145	0.325	0.007	0.311	0.340
EC_{80}	30.9	3.1	24.8	36.9	0.969	0.040	0.888	1.050

Table S5. Ecotoxicological effects reported in the literature for GO on photosynthetic microalgae.

Organism	**Size range**	**Exposure conditions**	**Toxicological effects**	**Reference**
Chlorella vulgaris	Thickness: 0.8–1 nm Diameter: 1–5 µm Size distribution: 465–486 nm	0.01, 0.1, 1, and 10 mg L^{-1} for 8 days.	- Cell growth inhibition and decrease in chlorophyll content as the concentrations of GO increased. - Generation of ROS and disrupted antioxidant enzymes. - GO enveloped and entered algal cells, and damaged organelles (especially via plasmolysis and an increase in the starch grain number).	Hu *et al*.[1]
	Thickness: 0.8–1.2 nm Lateral length: 0.5–5 µm Hydrodynamic diameter: 295–825 nm	0.01, 0.1, 1, and 10 mg L^{-1} for 96 h.	- Cell division was promoted at 24 h and then inhibited at 96 h. - GO promoted the generation of ROS, loss of mitochondrial membrane potential, plasmolysis and increases in the number of starch grains and the number of lysosome. - GO covered cell surface.	Hu *et al*.[2]
	Thickness: 0.1-1 nm Lateral length: 1.5 µm	0.01, 0.1, 1, and 10 mg L^{-1} for 96 h.	- Inhibition of cell division. - Increased intracellular ROS and mitochondrial membrane potential. - Internalization of GO, damaged the cell ultrastructure, reduced cell permeability, and plasmolysis.	Ouyang *et al*.[3]
	Thickness: 1.02 ± 0.15 nm Lateral length: 0.5–5 µm	0.1, 1 and 10 mg L^{-1} for 96 h	- Inhibition of cell division and chlorophyll *a* biosynthesis. - Enhancement of ROS. Oxidative stress-induced membrane damage, and nutrient depletion. - Cell plasmolysis.	Hu *et al*.[4]

Chlorella pyrenoidosa	Thickness: 2.1 nm Lateral size: 2 μm	50, 100, 150, 200 mg L^{-1} for 96 h	- Growth inhibition (EC_{50} 37.3 mg L^{-1}). - Increase of intracellular ROS and membrane damage.	Zhao *et al.*[5]
Picochlorum sp.	Thickness: 3-6 nm	0.5, 1, 2.5, and 5.0 mg L^{-1} for 32 days	- Decrease in viable cell number and chlorophyll *a* concentration. - GO formed a coating layer around algal cells and penetrated the cells without a significant change in their structure.	Hazeem *et al.*[6]
Raphidocelis subcapitata	Thickness: 3.5 nm. Hydrodynamic diameter: 110 nm	0.5, 2, 5, 10, 20, 50, 70, and 100 mg L^{-1} for 96 h.	- Growth inhibition (EC_{50} 20 mg L^{-1}). - Decrease in percentage of the chlorophyll autofluorescence intensity. - Oxidative stress and membrane integrity damage.	Nogueira *et al.*[7]
Scenedesmus obliquus	Thickness: 0.7 nm. Size: 1-10 μm.	1, 2, 4, 8, 16, 32, and 64 mg L^{-1} for 96 h (Combined exposure to GO and Cu^{2+} for 96 h and 12 days.	- Growth inhibition (EC_{50} 21.2 ± 0.5 mg L^{-1}). - Antagonistic effects between GO and copper. GO reduce ecotoxicity of Cu^{2+} at low and environmentally relevant concentrations.	Hu *et al.*[8]

1. X. Hu, K. Lu, L. Mu, J. Kang and Q. Zhou, *Carbon*, 2014, **80**, 665-676.
2. X. Hu, S. Ouyang, L. Mu, J. An and Q. Zhou, *Environmental Science & Technology*, 2015, **49**, 10825-10833.
3. S. Ouyang, X. Hu and Q. Zhou, *ACS Applied Materials & Interfaces*, 2015, **7**, 18104-18112.
4. X. Hu, Y. Gao and Z. Fang, *Carbon*, 2016, **109**, 65-73.
5. J. Zhao, X. Cao, Z. Wang, Y. Dai and B. Xing, *Water Research*, 2017, **111**, 18-27.
6. L. J. Hazeem, M. Bououdina, E. Dewailly, C. Slomianny, A. Barras, Y. Coffinier, S. Szunerits and R. Boukherroub, *Environmental Science and Pollution Research*, 2017, **24**, 4144-4152.
7. P. F. M. Nogueira, D. Nakabayashi and V. Zucolotto, *Aquatic Toxicology*, 2015, **166**, 29-35.
8. C. Hu, N. Hu, X. Li and Y. Zhao, *Ecotoxicology and Environmental Safety*, 2016, **132**, 360-365.

Table S6. Dose-effect relationship parameters of GO, and wastewater (WW) individually and of their binary combinations on *C. reinhardtii* after 72 h of exposure.

	Drug combo	Dose-Effect parameters		
		D_m	m	r
Constant ratio	GO	1.31	0.61	0.953
	WW	0.34	1.04	0.970
	GO+WW	1.35	1.34	0.976
Non-constant ratio	GO	1.64	0.64	0.923
	WW	0.62	0.54	0.932
	GO+WW	1.16	2.48	0.964

The parameters m, D_m and r are the antilog of x-intercept, the slope and the linear correlation coefficient of the median-effect plot, which signifies the shape of the dose-effect curve, the potency (EC_{50}), and conformity of the data to the mass-action law, respectively. m was the Hill coefficient used to determine the shape of the dose-response curve, hyperbolic ($m = 1$), sigmoidal ($m > 1$) or negative sigmoidal ($m < 1$); also shown in the table, linear regression correlation coefficients (r-values) of the median-effect plots were > 0.90 in all cases, indicating the conformity of the data to the median-effect principle.

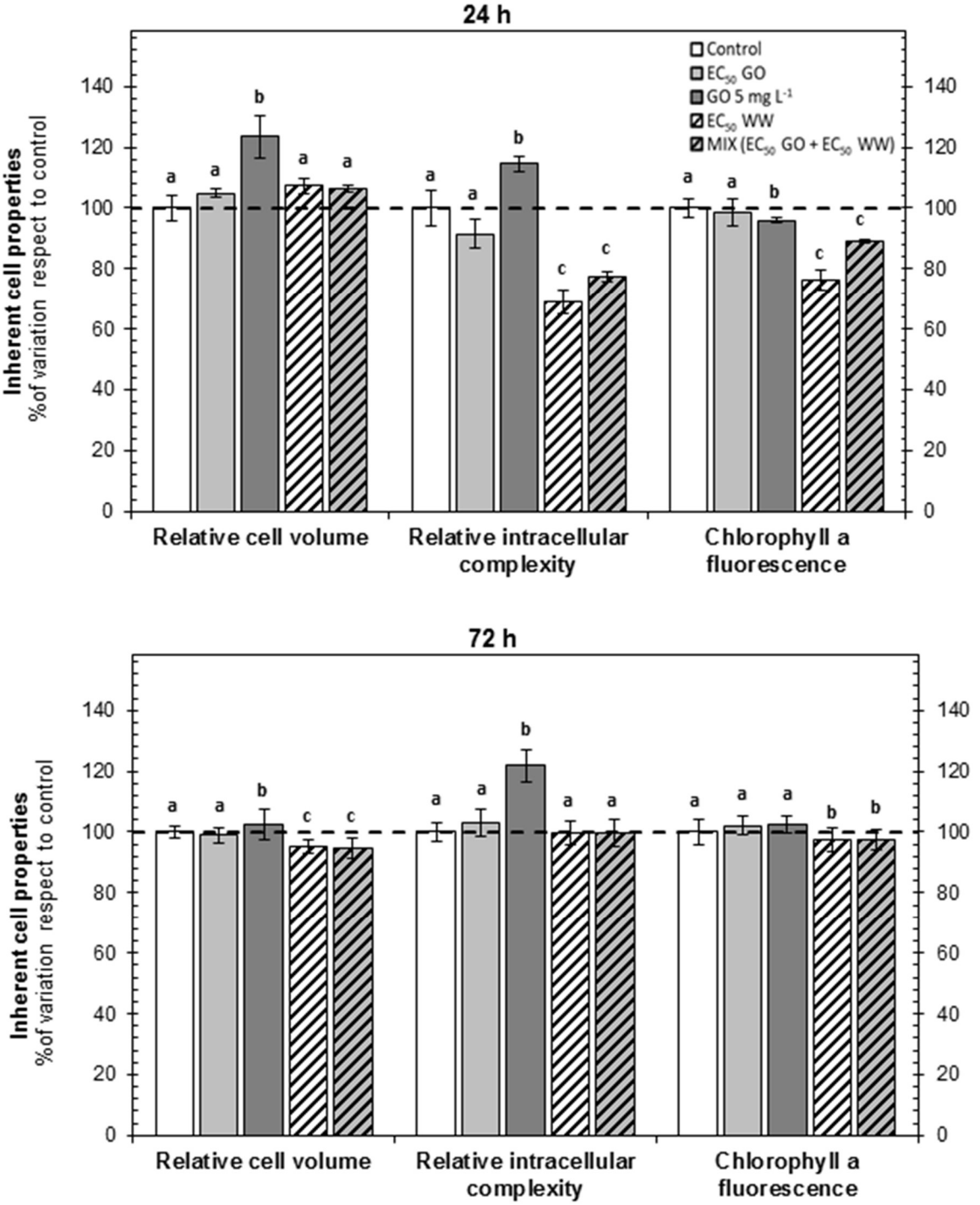

Figure S3. Variations in inherent cell properties of *C. reinhardtii* cells after 24 and 72 h of exposure. Results are shown as percentage of variation of cell volume, intracellular complexity, and chlorophyll *a* fluorescence ± SD with respect to control (assigned a value of 100%, indicated by the dashed line). Treatments with different letters are significantly different (Tukey's´ HSD, $p < 0.01$).

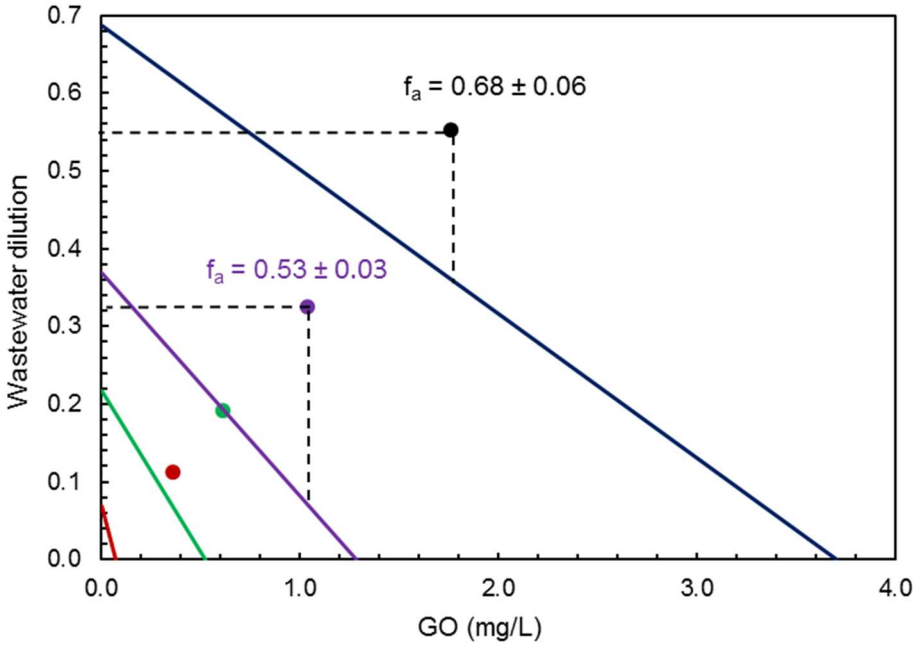

Figure S4. Isobolograms representing constant ratio binary combinations for different joint affected fraction (f_a). Vertical distances represent the wastewater dilution theoretically required to reach additivity. Points with the same colour represent experimental toxicity and error.

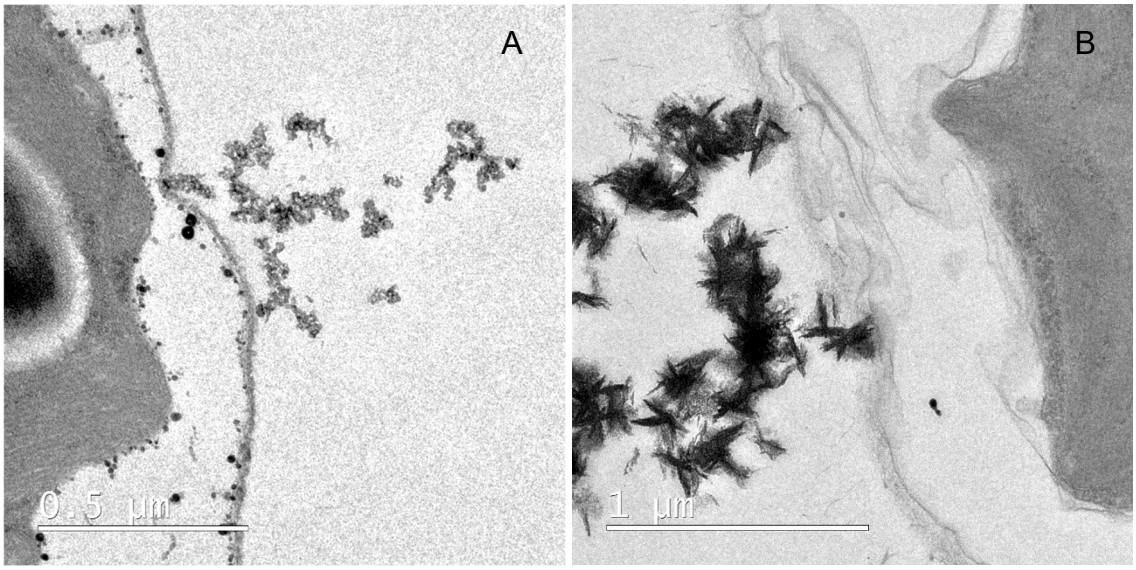

Figure S5. TEM micrographs of *C. reinhardtii* (A) exposed to 5 mg L^{-1} GO in Tris-minimal phosphate (TP) medium at pH 6.5 and (B) in wastewater at EC_{50} GO + EC_{50} wastewater for 72 h.

Table S7. Experimental results related to the data points shown in Fig. 1.

Constant ratio					
Data point	GO (mg/L)	WW dil.	f_a	CI	CI SD
1	0.358	0.112	0.173	5.20	0.71
2	0.609	0.191	0.379	1.96	0.40
3	1.036	0.325	0.499	1.73	0.31
4	1.761	0.552	0.685	1.16	0.25
5	2.994	0.939	0.799	0.98	0.23
Non-constant ratio					
Data point	GO (mg/L)	WW dil.	f_a	CI	CI SD
1	0.173	0.271	0.087	37.8	4.9
2	0.345	0.217	0.123	18.9	4.8
3	0.518	0.163	0.192	6.96	1.37
4	0.691	0.108	0.271	3.08	0.43
5	0.863	0.054	0.350	1.56	0.21